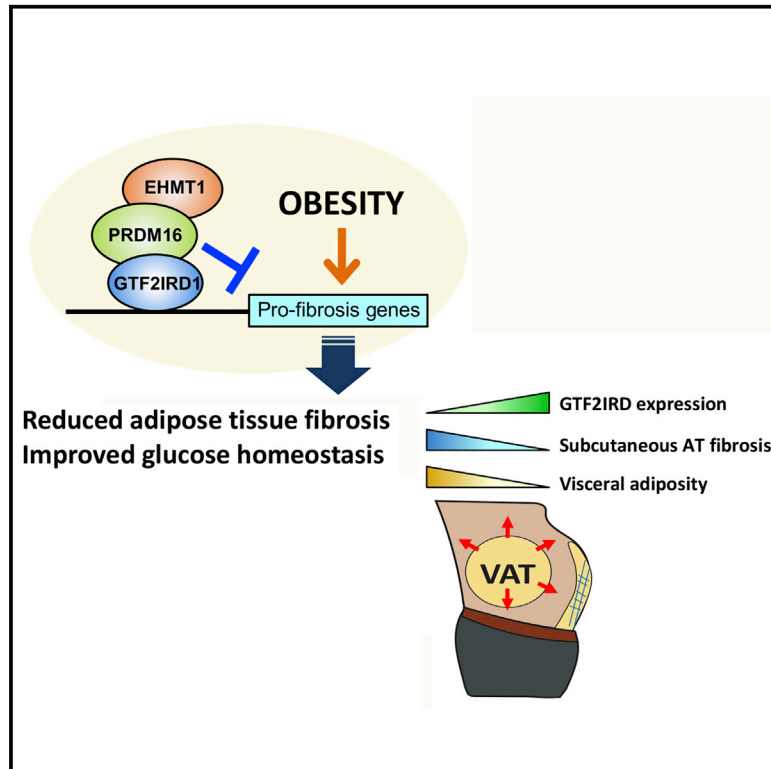


Cell Metabolism

Repression of Adipose Tissue Fibrosis through a PRDM16-GTF2IRD1 Complex Improves Systemic Glucose Homeostasis

Graphical Abstract



Authors

Yutaka Hasegawa, Kenji Ikeda,
Yong Chen, ..., Paul Cohen,
Suneil K. Koliwad, Shingo Kajimura

Correspondence

suneil.koliwad2@ucsf.edu (S.K.K.),
shingo.kajimura@ucsf.edu (S.K.)

In Brief

Hasegawa et al. identify GTF2IRD1 as a cold-inducible transcription factor that represses adipose tissue fibrosis through a PRDM16-EHMT1 complex. Repression of adipose tissue fibrosis by the complex improves systemic glucose homeostasis independent of UCP1-mediated thermogenesis and body weight. In humans, GTF2IRD1 expression inversely correlates with subcutaneous WAT fibrosis and visceral adiposity.

Highlights

- GTF2IRD1 is a transcription factor that forms a complex with PRDM16 and EHMT1
- A PRDM16-GTF2IRD1 complex cell-autonomously represses adipose tissue fibrosis
- Repression of adipose tissue fibrosis improves systemic glucose homeostasis
- GTF2IRD1 expression inversely correlates with subcutaneous WAT fibrosis in humans



Repression of Adipose Tissue Fibrosis through a PRDM16-GTF2IRD1 Complex Improves Systemic Glucose Homeostasis

Yutaka Hasegawa,^{1,2,3,6} Kenji Ikeda,^{1,2,3,8} Yong Chen,^{1,2,3,8} Diana L. Alba,^{1,4,8} Daniel Stifler,^{1,4} Kosaku Shinoda,^{1,2,3} Takashi Hosono,^{1,2,3,7} Pema Maretich,^{1,2,3} Yangyu Yang,^{1,2,3} Yasushi Ishigaki,⁶ Jingyi Chi,⁵ Paul Cohen,⁵ Suneil K. Koliwad,^{1,4,*} and Shingo Kajimura^{1,2,3,9,*}

¹UCSF Diabetes Center, San Francisco, CA, USA

²Eli and Edythe Broad Center of Regeneration Medicine and Stem Cell Research, San Francisco, CA, USA

³Department of Cell and Tissue Biology, University of California, San Francisco, San Francisco, CA, USA

⁴Department of Medicine, University of California, San Francisco, San Francisco, CA, USA

⁵The Rockefeller University, Laboratory of Molecular Metabolism, New York, NY, USA

⁶Division of Diabetes and Metabolism, Department of Internal Medicine, Iwate Medical University, Morioka, Uchimaruru, Japan

⁷Department of Chemistry and Life Science, College of Bioresource Sciences, Nihon University, Tokyo, Japan

⁸These authors contributed equally

⁹Lead Contact

*Correspondence: suneil.koliwad2@ucsf.edu (S.K.K.), shingo.kajimura@ucsf.edu (S.K.)

<https://doi.org/10.1016/j.cmet.2017.12.005>

SUMMARY

Adipose tissue fibrosis is a hallmark of malfunction that is linked to insulin resistance and type 2 diabetes; however, what regulates this process remains unclear. Here we show that the PRDM16 transcriptional complex, a dominant activator of brown/beige adipocyte development, potently represses adipose tissue fibrosis in an uncoupling protein 1 (UCP1)-independent manner. By purifying the PRDM16 complex, we identified GTF2IRD1, a member of the TFII-I family of DNA-binding proteins, as a cold-inducible transcription factor that mediates the repressive action of the PRDM16 complex on fibrosis. Adipocyte-selective expression of GTF2IRD1 represses adipose tissue fibrosis and improves systemic glucose homeostasis independent of body-weight loss, while deleting GTF2IRD1 promotes fibrosis in a cell-autonomous manner. GTF2IRD1 represses the transcription of transforming growth factor β -dependent pro-fibrosis genes by recruiting PRDM16 and EHMT1 onto their promoter/enhancer regions. These results suggest a mechanism by which repression of obesity-associated adipose tissue fibrosis through the PRDM16 complex leads to an improvement in systemic glucose homeostasis.

INTRODUCTION

Dysregulation of adipose tissue homeostasis is a primary cause of obesity-related metabolic disorders, including insulin resistance, hepatic steatosis, and diabetes mellitus (Crews et al.,

2017). Mounting evidence highlights the importance of the extracellular matrix (ECM) in maintaining adipose tissue homeostasis. The accumulation of ECM proteins (e.g., collagens) during the early stages of obesity is a part of the tissue remodeling process that accompanies healthy adipose expansion; however, pathologically excessive accumulation of the ECM in adipose tissues causes fibrosis, which is tightly associated with the increased infiltration of pro-inflammatory immune cells into the adipose tissues, and subsequently greater tissue inflammation (Sun et al., 2013b). Importantly, such changes to the ECM, and consequent fibrosis in human subcutaneous white adipose tissue (WAT) are strongly linked to insulin resistance and type 2 diabetes (Divoux et al., 2010; Henegar et al., 2008; Lackey et al., 2014; Muir et al., 2016; Reggio et al., 2016). For instance, collagen VI (Col6), a major ECM protein in adipose tissues, accumulates at much higher rates under obese and diabetic states (Dankel et al., 2014; Divoux et al., 2010; Khan et al., 2009; Pasarica et al., 2009; Spencer et al., 2010). In the absence of Col6, the WAT of obese mice is able to expand with less tissue fibrosis and inflammation; thus, the Col6-deficient mice display improved glucose tolerance and insulin sensitivity (Khan et al., 2009).

Two prominent pathways have been highlighted with regard to regulating adipose fibrosis: hypoxia-inducible factor 1 α (HIF1 α) and transforming growth factor β (TGF- β). In obesity, adipose tissue hypoxia results in the activation of HIF1 α -dependent gene transcription (Hosogai et al., 2007; Rausch et al., 2008; Ye et al., 2007). Moreover, mouse models with ectopic activation of HIF1 α in adipose tissues induce fibrosis and glucose intolerance (Halberg et al., 2009), whereas treatment with the HIF1 α -selective inhibitor PX-478 ameliorates adipose fibrosis, inflammation, and glucose intolerance (Sun et al., 2013a). Similarly, levels of TGF- β , a primary factor promoting tissue fibrosis, are highly elevated in both the circulation and adipose tissues of obese mice and humans (Samad et al., 1997; Yadav et al., 2011).

It is notable that TGF- β signaling exerts effects on brown/beige adipocyte biogenesis that are reciprocal to those on



adipose fibrosis. For example, TGF- β treatment of adipocyte precursor cells potently inhibits beige adipocyte differentiation and expression of uncoupling protein 1 (UCP1) (Koncarevic et al., 2012; McDonald et al., 2015). By contrast, inhibiting TGF- β signaling by genetic deletion of *Smad3*, or by a neutralizing antibody against the activin receptor type IIB, promotes brown and beige adipocyte biogenesis *in vivo* (Fournier et al., 2012; Koncarevic et al., 2012; Yadav et al., 2011). Furthermore, genetic ablation of myocardin-related transcription factor A, a G-actin-regulated transcriptional coactivator acting downstream of TGF- β signaling, has been shown to stimulate beige adipocyte differentiation (McDonald et al., 2015). The reciprocal relationship between adipose tissue fibrosis and brown/beige fat biogenesis may be simply due to body-weight loss through UCP1-mediated energy dissipation by brown and beige fat. However, our recent observations suggest that the improvements in systemic glucose homeostasis and reduced adipose tissue fibrosis, when beige adipocyte biogenesis is activated, are independent of body-weight loss and UCP1 expression. In fact, we recently found that transgenic mice expressing adipose tissue-selective PRDM16 (PR domain containing 16), which have an increased number of beige adipocytes in the subcutaneous WAT, have a remarkable improvement in glucose tolerance, and reduction in their susceptibility to diet-induced adipose tissue fibrosis independent of UCP1 (Ikeda et al., 2017).

As a part of the UCP1-independent mechanisms of beige fat action in the regulation of glucose homeostasis, the present study identifies GTF2IRD1, a member of the TFII-I family of DNA-binding transcription factor, which potently represses pro-fibrosis gene expression by forming a complex with PRDM16 and EHMT1. Notably, repression of adipose tissue fibrosis by the PRDM16-EHMT1-GTF2IRD1 complex leads to a significant improvement in systemic glucose homeostasis independent of UCP1-mediated thermogenesis and body-weight loss. Our data provide an exciting avenue of improving systemic glucose homeostasis *in vivo* by targeting adipose tissue fibrosis.

RESULTS

Repression of Adipose Tissue Fibrosis by PRDM16 Is UCP1-Independent

While transgenic mice expressing PRDM16 under control of the *Fabp4* promoter/enhancer have an increased number of beige adipocytes in the subcutaneous WAT in conjunction with improved glucose tolerance, PRDM16 transgenic mice (*Prdm16* Tg) fed a high-fat diet (HFD) for 10 weeks have improved systemic glucose tolerance even when crossed onto a UCP1-deficient background (Figure 1A). This improvement was significant before any difference in body-weight emerged between the two groups (Ikeda et al., 2017). These results suggest that the mechanism underlying enhanced systemic glucose tolerance in *Prdm16* Tg mice is not due to UCP1-mediated thermogenesis. Of note, we found that *Prdm16* Tg and *Prdm16* Tg x *Ucp1*^{-/-} mice had significantly less hydroxyproline, a biochemical marker of tissue fibrosis, in the inguinal WAT and the epididymal WAT relative to their respective controls (Figure 1B), in close conjunction with the improvement in systemic glucose tolerance. Masson's trichrome staining of WAT sections revealed that compared with corresponding littermates, *Prdm16*

Tg mice fed an HFD had far fewer trichrome-positive fibrotic streaks and similarly fewer crown-like structures, indicative of macrophages surrounding necrotic adipocytes (Figure 1C). Consistent with the observation of reduced hydroxyproline, the ability of adipocyte-specific *Prdm16* expression to limit WAT fibrosis and macrophage accumulation was preserved in the absence of UCP1. Similarly, immunostaining of WAT sections revealed that transgenic PRDM16 expression markedly reduced the expression of endotrophin, a C-terminal cleavage product of Col6 α 3 that stimulated WAT fibrosis (Park and Scherer, 2012; Sun et al., 2014), and that this effect too was independent of UCP1 (Figure 1D).

To understand the underlying mechanisms, we analyzed RNA-sequencing (RNA-seq) datasets of their inguinal WAT depots from these four genotypes. We found that a number of genes involved in connective tissue and ECM development were downregulated in *Prdm16* Tg and *Prdm16* Tg x *Ucp1*^{-/-} mice. Specifically, PRDM16 expression repressed genes encoding proteins comprising collagens, matrix metalloproteinases (*Mmps*), and *Lgals3* (encoding Galectin-3), which is implicated in the development of WAT fibrosis (Martinez-Martinez et al., 2016). Repression of these pro-fibrotic genes was seen in *Prdm16* Tg x *Ucp1*^{-/-} mice, indicating that this repression of adipose tissue fibrosis is independent of UCP1 (Figure 1E).

Notably, WAT fibrosis was also reduced in the inguinal WAT following chronic cold exposure. We found that mild cold exposure (16°C) for 10 days significantly reduced the expression of many pro-fibrosis genes in the inguinal WAT of wild-type mice and *Ucp1*^{-/-} mice (Figure 1F). Consistent with this observation, analysis of an independent microarray dataset (Xue et al., 2009) found that the expression of pro-fibrotic genes in the inguinal WAT was also downregulated by chronic cold exposure for both 1 and 5 weeks (Figure S1A). Together, these results indicate that both PRDM16 and chronic cold exposure potently represses molecular pathways involved in adipose tissue fibrosis through an UCP1-independent mechanism.

GTF2IRD1 Is a Cold-Inducible Transcription Factor that Forms a Transcriptional Complex with PRDM16 and EHMT1

Previous studies show that PRDM16 is recruited to brown/beige fat-specific genes through an interaction with DNA-binding transcription factors, such as peroxisome proliferator-activated receptors (PPARs), CCAAT-enhancer-binding proteins (C/EBPs), and early B cell factor 2 (EBF2) (Inagaki et al., 2016). However, the DNA-binding transcriptional factors that recruit the PRDM16 complex to the sites needed to regulate pro-fibrotic gene expression are unknown. Accordingly, we purified a PRDM16 transcriptional complex from the nuclear extracts of cultured beige adipocytes, and subsequently characterized the subunits by liquid chromatography coupled with tandem mass spectrometry. We identified 413 proteins as nuclear-localized transcriptional regulators, including the previously characterized factors CtBP1 and CtBP2, EHMT1, MED1, and p107 (Inagaki et al., 2016). We then cross-referenced this list with the annotated UniProt database, and found that the PRDM16 complex contains 43 DNA-binding transcriptional regulators, including C/EBP β , PPAR γ , EBF2, and ZFP516, as well as uncharacterized factors (Figure 2A; Table S1).

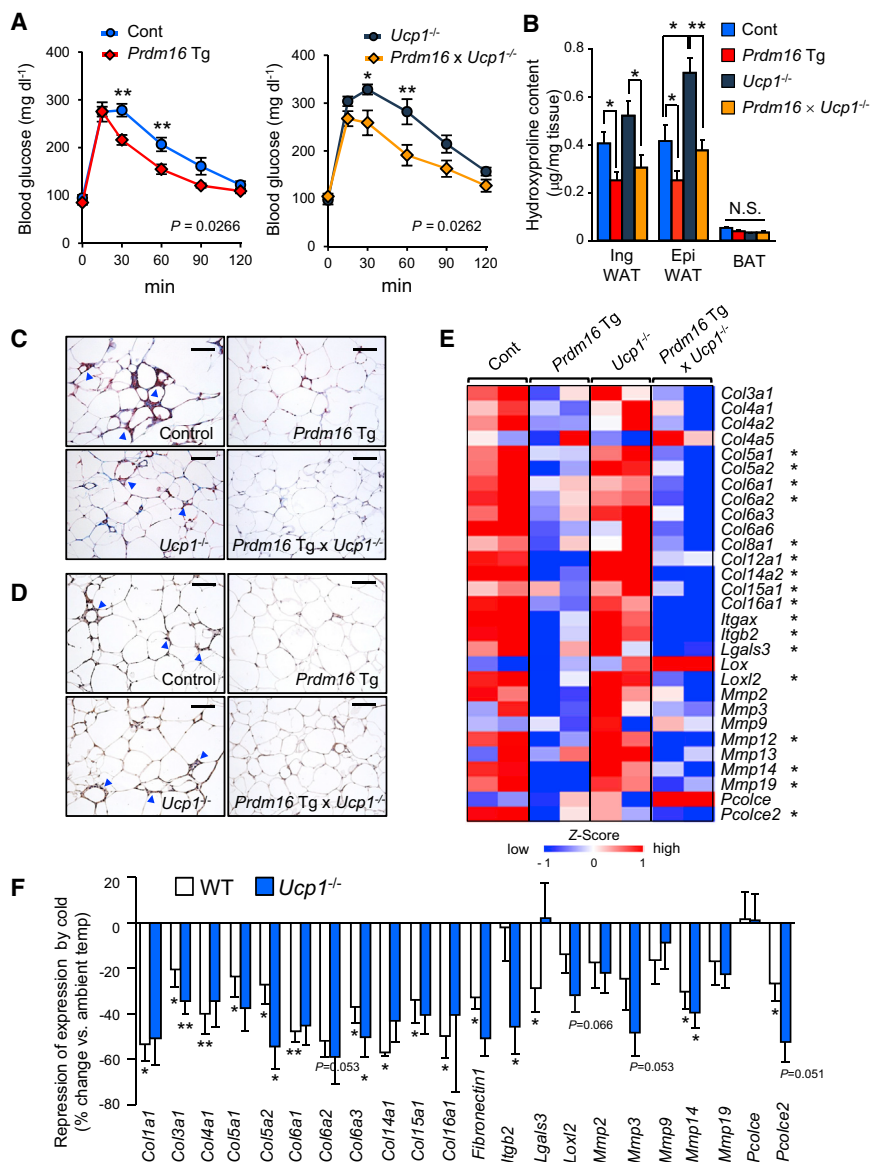


Figure 1. UCP1-Independent Regulation of Adipose Fibrosis by PRDM16

(A) Glucose tolerance test in *Prdm16* Tg mice and the littermate controls (left) and in *Ucp1*^{-/-} mice and *Prdm16* Tg x *Ucp1*^{-/-} mice (right) at 22°C. Mice were on a HFD for 10 weeks. n = 7–8. *p < 0.05, **p < 0.01.

(B) Hydroxyproline content in the BAT, the inguinal WAT, and the epididymal WAT of mice with indicated genotypes under HFD for 14 weeks. n = 6–10. *p < 0.05 between *Prdm16* Tg and controls as well as between *Prdm16* Tg x *Ucp1*^{-/-} and *Ucp1*^{-/-}.

(C) Masson's trichrome staining in the epididymal WAT of mice with indicated genotypes under HFD. Arrowheads indicate crown-like structures. Scale bars, 100 μm.

(D) Immunohistochemical staining with anti-mouse endothelin antibody in the epididymal WAT of mice in (C). Arrowheads indicate crown-like structures. Scale bars, 100 μm.

(E) Expression profiles of pro-fibrotic genes (as indicated) in the inguinal WAT of mice with indicated genotypes under HFD for 14 weeks. The color scale shows Z scored fragments per kilobase of transcript per million fragments mapped (FPKM) representing the mRNA level of each gene in blue (low expression)-white-red (high expression) scheme. *p < 0.05 by transgenic PRDM16 expression in both wild-type background and *Ucp1*^{-/-} background.

(F) Cold-induced changes in gene expression of pro-fibrosis genes (percent of change relative to ambient temperature) in the inguinal WAT from wild-type (white) and *Ucp1*^{-/-} mice (blue). Mice under 14 weeks of HFD were kept under ambient temperature or mild cold temperature at 16°C for 10 days. n = 4–6. *p < 0.05 relative to mice under ambient temperature.

Data in (A), (B), and (F) are represented as mean ± SEM.

Based on our transcriptome datasets (Shinoda et al., 2015), we found that ten transcription factors were specifically enriched in brown adipose tissue (BAT) (Figure 2B). Since adipose tissues are highly heterogeneous, we subsequently validated their expression levels in primary cultured brown adipocytes, and found that the mRNA levels of five transcription factors, *Gtf2ird1*, *Zfp148*, *Cebpb*, *Ebf2*, and *Zhx1*, were enriched in primary brown adipocytes than white adipocytes (Figure 2C). In this study, we focused on *Gtf2ird1* because of its clear co-enrichment with PRDM16 in mature brown adipocytes (Figures S1B and S1C), as well as its involvement in Williams-Beuren syndrome in which the *GTF2IRD1* gene is deleted in humans (Makeyev et al., 2004; Tipney et al., 2004).

Notably, exposing mice to temperatures under 6°C for 3 days significantly increased the levels of both *Gtf2ird1* mRNA (Figure 2D) and GTF2IRD1 protein (Figure 2E) in the BAT. Furthermore, daily systemic administration of a β3-adrenoceptor

(β3-AR) agonist (CL316,243) to wild-type mice for 7 days significantly increased *Gtf2ird1* mRNA levels in the BAT (Figure 2F). CL316,243 treatment also induced *Gtf2ird1* expression in inguinal WAT and epididymal WAT, although at levels lower than that induced in BAT. Since forskolin treatment also increased *Gtf2ird1* mRNA levels in cultured brown adipocytes (Figure S1D), β3-AR-dependent induction of *Gtf2ird1* is mediated, at least in part, by cyclic AMP signaling. Among 11 transcriptional variants of *Gtf2ird1* in mice, variant 5 appears to be a major *Gtf2ird1* transcript in BAT (Figures S1D and S1E).

We next investigated the interaction between GTF2RD1 and the PRDM16-EHMT1 complex; EHMT1 is a histone methyltransferase essential for PRDM16 function in brown and beige adipocyte development (Harms et al., 2014; Ohno et al., 2013). First, we detected endogenous GTF2IRD1 from the complexes that pulled down with purified EHMT1 extracted from the nuclei of differentiated adipocytes (Figure 2G). Next, *in vitro* binding assays using purified GTF2IRD1 and PRDM16 fragments fused to glutathione S-transferase found that GTF2IRD1 directly binds

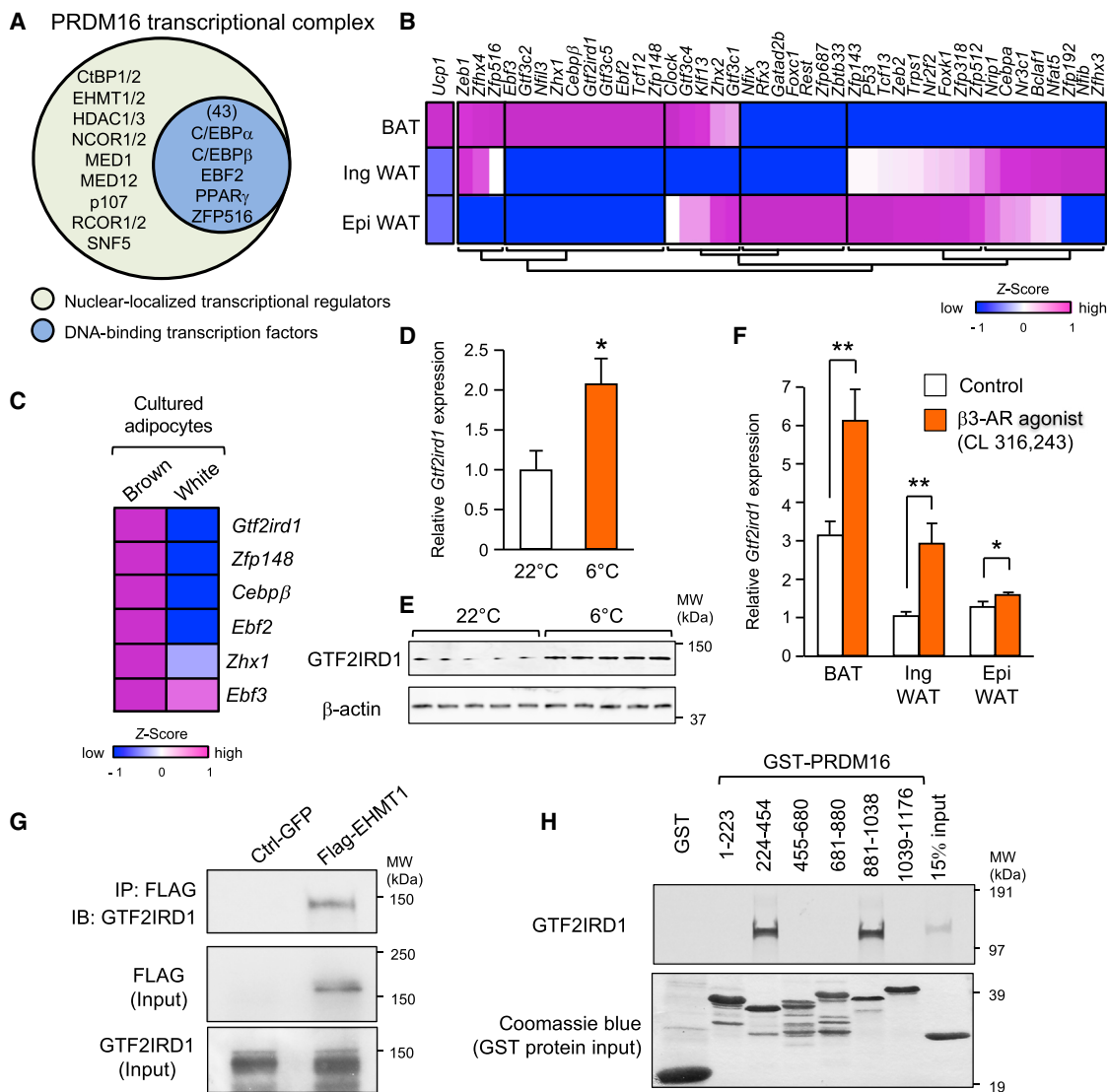


Figure 2. GTF2IRD1 Is a Cold-Inducible Transcription Factor that Forms a Complex with PRDM16 and EHMT1 in the BAT

(A) Identification of nuclear-localized components in a PRDM16 transcriptional complex purified from differentiated beige adipocytes. Nuclear-localized proteins and canonical DNA-binding transcription factors were listed based on the annotation database in UniProt.

(B) Gene expression profile of the identified transcriptional factors in interscapular BAT, inguinal WAT, and epididymal WAT. The color scale shows Z scored FPKM representing the mRNA level of each gene in blue (low expression)-white-red (high expression) scheme.

(C) Gene expression profile of the BAT-enriched transcriptional factors in cultured primary brown adipocytes and white adipocytes.

(D) Expression of *Gtf2ird1* in BAT from mice housed at 22°C or 6°C for 3 days. $n = 5$.

(E) Immunoblotting for GTF2IRD1 protein from mice in (D). β -actin was used as loading control.

(F) Expression of *Gtf2ird1* mRNA in the indicated adipose tissues of mice treated with vehicle (saline) or CL316, 243 at a dose of 1 mg/kg for 7 days. $n = 5$. * $p < 0.05$, ** $p < 0.01$. Data in (D) and (F) are represented as mean \pm SEM.

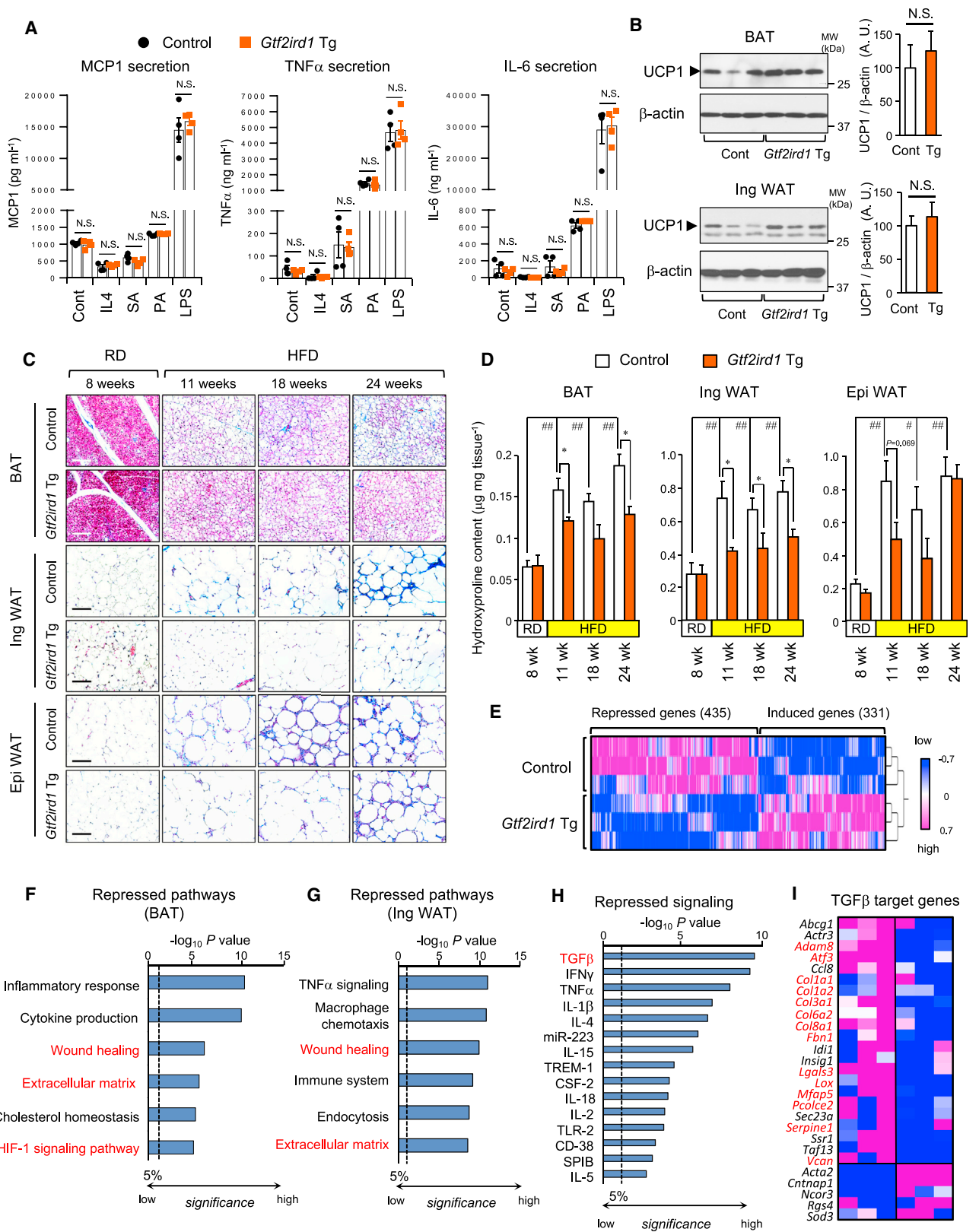
(G) A EHMT1 complex was immunopurified from differentiated brown adipocytes. Endogenous GTF2IRD1 was detected by immunoblotting. Inputs are shown in lower panels.

(H) *In vitro* binding assay of 35 S-labeled GTF2IRD1 and the indicated glutathione S-transferase (GST)-fusion fragments of PRDM16. Coomassie brilliant blue for GST-proteins (bottom panel).

to two distinct zinc-finger domains of PRDM16 domains, to which C/EBP β and PPAR γ are also known to bind (Kajimura et al., 2010) (Figure 2H). These results suggest that GTF2IRD1 is a cold-inducible and BAT-enriched transcriptional factor that interacts with both PRDM16 and EHMT1 to form a transcriptional complex.

Adipose-Selective Expression of GTF2IRD1 Represses Diet-Induced Adipose Tissue Fibrosis

To investigate the biological role of GTF2IRD1 *in vivo*, we generated transgenic mice in which variant 5 of *Gtf2ird1* is driven by the *Fabp4* promoter/enhancer in adipose tissues (*Gtf2ird1* Tg). We confirmed that *Gtf2ird1* mRNA and protein



(legend on next page)

expression levels in the BAT and WAT of *Gtf2ird1* Tg mice were significantly elevated compared with those of littermate controls (Figures S2A and S2B). Since a transgene driven by the *Fabp4* promoter/enhancer can be detected in non-adipocytes, including macrophages (Lee et al., 2013), we first determined if macrophage activation is altered by transgenic *Gtf2ird1* expression. To this end, we examined pro-inflammatory responses in the isolated macrophages from *Gtf2ird1* Tg and the littermate controls by measuring pro-inflammatory cytokines (monocyte chemoattractant protein-1, tumor necrosis factor alpha [TNF- α], and interleukin-6 [IL-6]) following treatment with pro-inflammatory stimuli, such as IL-4, stearic acid, palmitic acid, and lipopolysaccharide. The assays found no significant differences in cytokine production and release in macrophages from *Gtf2ird1* Tg and control mice (Figures 3A and S2C). Thus, a specific contribution of macrophages to the differential regulation of tissue inflammatory response appears negligible in this animal model.

Next, we asked if *Gtf2ird1* Tg mice have an altered adipose tissue thermogenesis *in vivo*. We found no difference in the level of UCP1 protein expressed in either the BAT or the inguinal WAT between *Gtf2ird1* Tg mice and the littermate controls (Figure 3B). *Gtf2ird1* Tg and control mice also displayed similar mRNA levels of the thermogenic genes in the BAT and the inguinal WAT, and whole-body heat production (Figures S2D–S2H). However, *Gtf2ird1* Tg mice displayed far fewer developed fibrotic structures in the adipose tissue on a HFD. While trichrome staining detected very few fibrotic structures in the adipose tissue on a regular diet (RD), fibrotic structures gradually developed after 11 weeks of HFD or longer in the WAT and the BAT, with the most severe fibrosis in the epididymal WAT (Figure 3C). We found significantly less fibrosis in the BAT and the inguinal WAT of *Gtf2ird1* Tg mice relative to littermate controls at all the time points examined on a HFD. Fewer fibrotic structures were also found in the epididymal WAT of *Gtf2ird1* Tg mice than control mice at 11 weeks of HFD; however, the difference was not obvious following longer periods of HFD. A similar trend was found when the adipose tissues were stained with picrosirius staining (Figure S3A). In addition, quantification of hydroxyproline contents in the adipose tissue showed that the BAT and the inguinal WAT of *Gtf2ird1* Tg mice were significantly less fibrotic than the controls at 11 weeks of HFD and thereafter, although no difference was seen on a RD (Figure 3D). There

was a trend toward reduced fibrosis in the epididymal WAT of *Gtf2ird1* Tg mice at 11 weeks of HFD, but no significant difference was seen at later time points of HFD.

We next performed RNA-seq analysis in the adipose tissue of *Gtf2ird1* Tg mice at 18 weeks of HFD. Hierarchical clustering of the RNA-seq data showed that the expression of 435 genes was significantly decreased, and that of 331 genes was significantly increased in the iBAT of *Gtf2ird1* Tg versus the littermate controls (Figure 3E). The Metascape biological pathway analysis indicates that pro-inflammatory pathways, including inflammatory responses, cytokine production, TNF- α signaling, and macrophage chemotaxis, were significantly reduced in the BAT and the WAT of *Gtf2ird1* Tg mice relative to control mice (Figures 3F, 3G, and S3B). Consistent with the histological observations, biological pathways involved in adipose tissue fibrosis, including “wound healing,” “extracellular matrix,” and “HIF1-signaling,” were significantly repressed in the BAT and WAT of *Gtf2ird1* Tg mice. Next, we applied Ingenuity pathway analysis to the RNA-seq dataset to identify signaling pathways upstream of GTF2IRD1-regulated biological processes. The analysis suggests that *Gtf2ird1* Tg mice had significantly reduced expression of genes involved in pro-inflammatory cytokine-driven signaling pathways, including but not limited to those induced by interferon- γ , TNF- α , IL-1 β , and IL-4 (Figure 3H). These data support the above observation that GTF2IRD1 represses adipose inflammation at 18 weeks of HFD *in vivo*. Among these signaling pathways, the TGF- β pathway was most strongly repressed in *Gtf2ird1* Tg mice. We then probed GTF2IRD1-repression of TGF- β -dependent signaling more closely due to this strong repression, and also because TGF- β is a well-known inducer of fibrosis in many peripheral organs, including lung, adipose tissues, and liver (Meng et al., 2016). In fact, a large component of TGF- β -regulated genes (22/27, 81.5%), many of which (highlighted by red letters) implicated in tissue fibrosis, were repressed in *Gtf2ird1* Tg mice relative to controls (Figure 3I). This change was independent of alterations in lipid metabolism, because no change was found in the expression of genes involved in *de novo* lipogenesis or lipolysis between the two groups (Figure S3C). Together, these data suggest that GTF2IRD1 represses HFD-induced adipose tissue fibrosis, in part, through inhibiting TGF- β -dependent pro-fibrotic signaling pathways *in vivo*.

Figure 3. Adipose-Selective Expression of *Gtf2ird1* Represses Adipose Tissue Fibrosis *In Vivo*

- (A) Concentration of monocyte chemoattractant protein-1 (MCP-1), TNF- α , and IL-6 secreted from the macrophages from *Gtf2ird1* Tg mice and the littermate control mice (control). The isolated macrophages were stimulated with IL-4, stearic acid (SA), palmitic acid (PA), or lipopolysaccharide (LPS). $n = 4$.
- (B) Immunoblotting for UCP1 in the BAT (upper panel) and the inguinal WAT (bottom panel) from *Gtf2ird1* Tg mice and controls under ambient temperature. $n = 6$ –7. β -actin was used as loading control. Quantification of the UCP1 signal normalized by β -actin is shown on the right graphs. N.S., not significant.
- (C) Masson's trichrome staining in the BAT, the WAT, and the epididymal WAT from *Gtf2ird1* Tg and controls on 8 weeks of RD or HFD for 11, 18, and 24 weeks. Scale bars, 100 μ m.
- (D) Hydroxyproline content in the adipose tissues of mice in (C). * $p < 0.05$ between *Gtf2ird1* Tg mice and controls. # $p < 0.05$, ## $p < 0.01$ between RD and HFD. $n = 5$. Data in (A), (B), and (D) are represented as mean \pm SEM.
- (E) Hierarchical clustering and heatmap of RNA-seq transcriptome in the BAT of control and *Gtf2ird1* Tg mice. The color scale shows Z scored FPKM representing the mRNA level of each gene in blue (low expression)-white-red (high expression) scheme.
- (F) Repressed biological pathways in the BAT of *Gtf2ird1* Tg mice and controls by Metascape.
- (G) Repressed biological pathways in the inguinal WAT of *Gtf2ird1* Tg mice and controls by Metascape.
- (H) Ingenuity upstream analysis identified repressed signaling pathways in the BAT of *Gtf2ird1* Tg mice.
- (I) Expression profiles of the TGF- β -regulated genes in the BAT of control and *Gtf2ird1* Tg mice. Genes with red letters represent pro-fibrosis genes.

A Cell-Autonomous Function of GTF2IRD1 for Inhibiting Adipocyte Fibrosis

Based on the close alignment between the reduced adipose tissue fibrosis in *Gtf2ird1* Tg mice and the role of TGF- β signaling in the regulation of adipose fibrosis, we asked whether GTF2IRD1 is required, cell-autonomously, for the fibrotic responsiveness of adipocytes. We thus transduced retroviruses expressing either a scrambled control RNA (scr) or small hairpin RNAs (shRNAs) targeting *Gtf2ird1* (sh-*Gtf2ird1* no. 1 or no. 2) into immortalized brown adipocytes (Figure 4A). To induce fibrosis in cultured adipocytes, the transduced cells were then treated with TGF- β at doses of 0.2, 1.0, or 5.0 ng/mL under pro-adipogenic conditions. Consistent with prior work (Choy and Derynck, 2003), TGF- β treatment potently and dose-dependently impaired adipogenesis, whereas adipogenesis was impaired even at baseline when GTF2IRD1 was knocked down, and this impairment was further enhanced when the cells were treated with TGF- β (Figure 4B). GTF2IRD1 depletion also reduced the mRNA levels of BAT-specific genes, including *Ucp1*, *Elovl3*, and *Cidea* (Figure 4C), likely a reflection of impaired adipogenesis. In contrast, GTF2IRD1 depletion was associated with the induction of several pro-fibrotic genes, such as *Col3a1*, *Lgals3* (encoding Galectin-3), *Pcolce2*, *Mmp2*, and *Fibronectin1* and this induction was further enhanced in the presence of TGF- β (Figures 4D and S4A). In contrast, no significant change was found in the expression of pro-inflammatory genes by GTF2IRD1 depletion (Figure S4B).

We next employed gain-of-function approaches to ask if GTF2IRD1 represses adipocyte fibrosis in response to TGF- β signaling. First, we overexpressed a retroviral FLAG-tagged GTF2IRD1 construct in immortalized brown preadipocytes and subsequently treated with either TGF- β or vehicle to stimulate cellular fibrosis (Figure S4C). We found that overexpressing GTF2IRD1 potently diminished the ability of TGF- β to increase mRNA levels of the pro-fibrotic genes *Lgals3* and *Pcolce2* (Figure S4E), whereas no change was found in the expression of pro-inflammatory genes (Figure S4D). To recapitulate the conditions of *Gtf2ird1* Tg BAT in culture, we next isolated primary SVFs from the BAT of *Gtf2ird1* Tg mice and controls, and then differentiated these cells in the presence of TGF- β . Similarly, we found that primary brown adipocytes from *Gtf2ird1* Tg mice expressed significantly less pro-fibrosis genes than those from the littermate control mice, whereas no significant difference was found in the expression of genes involved in thermogenesis or inflammation between the two groups (Figure 4F). Of note, we found that GTF2IRD1 also repressed pro-fibrosis genes in *Ucp1*^{-/-} brown adipocytes (Figure S4E), as well as even when overexpressed in mature adipocytes by adenovirus (Figures S4F–S4J). Collectively, these data suggest that GTF2IRD1 negatively controls adipocyte fibrosis in a cell-autonomous manner, whereas GTF2IRD1 does not directly regulate the expression of thermogenesis genes or pro-inflammatory genes.

Regulatory Mechanisms of Pro-fibrosis Gene Expression by GTF2IRD1 in Mice and Humans

The above results led us to hypothesize that GTF2IRD1 transcriptionally represses cellular fibrosis by recruiting the PRDM16-EHMT1 complex onto the promoter/enhancer regions

of pro-fibrosis genes. To test this hypothesis, we first searched for the 8-bp core consensus binding motif sequence for GTF2IRD1, (G/A)GATT(A/G) (Chimge et al., 2008; Thompson et al., 2007) in the regulatory regions of two representative TGF- β -regulated pro-fibrotic genes, *Lgals3* and *Pcolce2* (Figures 5A and S5A). Among three potential sites on each gene, chromatin immunoprecipitation (ChIP) assays showed that GTF2IRD1 was significantly enriched at the regulatory regions of *Lgals3* and *Pcolce2* at sites A and D, respectively. Importantly, EHMT1 was co-enriched at these same sites (Figures 5B and S5B). In addition, from a previous dataset, which employed ChIP-sequencing for PRDM16 (Harms et al., 2015), we found that PRDM16 was also enriched at loci corresponding with *Lgals3* (Figure 5C).

We next asked if the GTF2IRD1-mediated repression of pro-fibrosis transcription requires the PRDM16-EHMT1 complex. To this end, we overexpressed GTF2IRD1 in immortalized adipocytes from *Prdm16*^{-/-} mice. We found that GTF2IRD1 failed to repress many of the pro-fibrosis genes in *Prdm16*^{-/-} cells (Figure 5D). Furthermore, adipocytes lacking PRDM16 or EHMT1 exhibited a similar phenotype to GTF2IRD1-depleted adipocytes: adipocytes from *Prdm16*^{-/-} mice and *Ehmt1*-knockdown cells expressed higher expression of pro-fibrotic genes in the presence of TGF- β (Figures S5C and S5D). In addition, pathway analyses of the global transcriptome datasets from inguinal WAT depots of adipocyte-specific *Prdm16*^{-/-} mice (Cohen et al., 2014) and adipocyte-specific *Ehmt1*^{-/-} mice (Ohno et al., 2013) showed that ECMs and pro-fibrosis genes were upregulated in both knockout mice relative to their respective controls (Figures S5E and S5F). These results suggest a functional requirement of the PRDM16-EHMT1-GTF2IRD1 complex to repress pro-fibrosis gene expression.

Next, we sought to determine whether the tissue-specific reciprocal relationship between *Gtf2ird1* expression and that of genes involved in adipose tissue fibrosis seen in mice is mirrored in human subjects. We examined human subcutaneous WAT samples from individuals with varying degrees of obesity recruited from a multiethnic cohort of adults assembled in the San Francisco Bay Area. Examining a mixed population of Caucasian individuals and those of Chinese ethnicity revealed an overall positive correlation between increasing visceral adiposity by DEXA and increasing mRNA levels of genes indicative of WAT fibrosis, such as *COL1A1*, *COL3A1*, *COL6A1*, *LGALS3*, *MMP2*, and *TIMP1* (Figures 5E and S5G). By contrast, mRNA levels of *GTF2IRD1* in the subcutaneous WAT of the same individuals showed an inverse correlation with visceral adiposity and body mass index (Figures 5F and 5G). In addition, *PRDM16* mRNA levels in the subcutaneous WAT displayed an inverse correlation with visceral WAT mass (Figure S5H). Remarkably, placing the individuals into groups reflecting relatively high versus low expression of *GTF2IRD1* revealed that those with high *GTF2IRD1* expression had lower expression of pro-fibrotic genes in the subcutaneous WAT (Figure 5H). This reduction was significant for *COL1A1*, *COL6A1*, *MMP2*, *LGALS3*, and *TIMP1*, and was a consistent trend for *COL3A1* ($p = 0.08$), although not statistically significant. This reciprocal relationship in humans mirrors that seen in both cultured adipocytes and adipose tissues in mice.

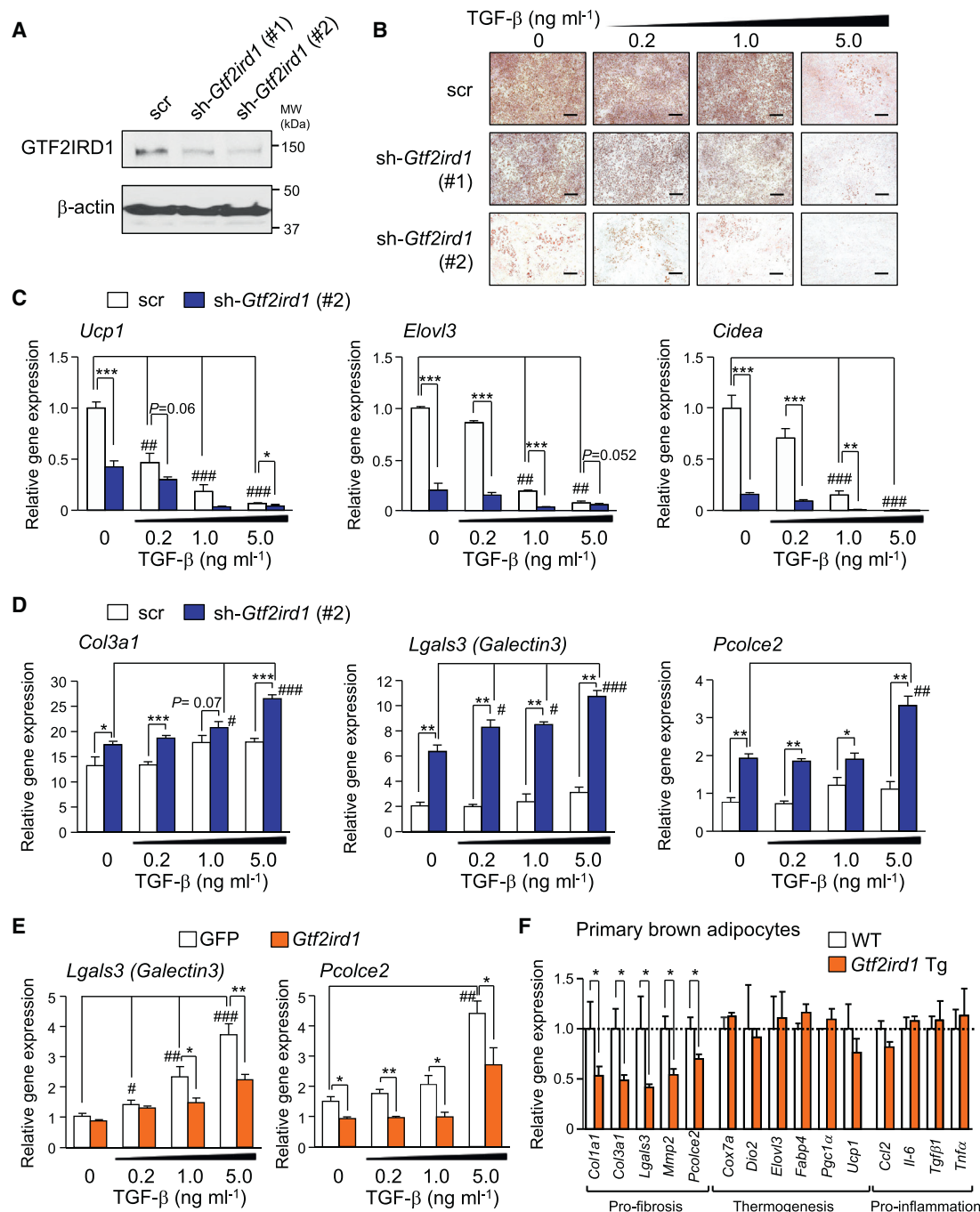


Figure 4. GTF2IRD1 Is Required for the Cell-Autonomous Capacity to Regulate Adipocyte Fibrosis

(A) Immunoblotting of immortalized brown adipocytes expressing shRNAs for a scrambled control (scr) or GTF2IRD1 (sh-*Gtf2ird1* no. 1 and no. 2). β -actin was used as loading control.

(B) Oil red O staining of brown adipocytes expressing scr or sh-*Gtf2ird1* cultured under an adipogenic condition medium containing TGF- β at 0.2, 1.0, or 5.0 ng mL⁻¹. Scale bars, 200 μ m.

(C) Relative mRNA expression of the BAT-related genes by qRT-PCR. * p < 0.05, ** p < 0.01, *** p < 0.001 between scrambled control and sh-*Gtf2ird1*. # p < 0.05, ## p < 0.01, ### p < 0.001 between the vehicle and TGF- β . n = 4.

(D) Relative mRNA expression of pro-fibrosis genes in (C).

(E) Relative mRNA expression of pro-fibrosis genes in immortalized brown adipocytes expressing GFP control or GTF2IRD1. * p < 0.05, ** p < 0.01 between GFP and *Gtf2ird1*. # p < 0.05, ## p < 0.01, ### p < 0.001 between vehicle and TGF- β . n = 4.

(F) Relative mRNA expression of pro-fibrosis genes, thermogenic genes, and pro-inflammatory genes in primary brown adipocytes derived from *Gtf2ird1* Tg mice and control mice. Cells were treated with TGF- β to induce fibrosis. * p < 0.05 between WT and *Gtf2ird1* Tg. n = 4.

Data in (C)–(F) are represented as mean \pm SEM.

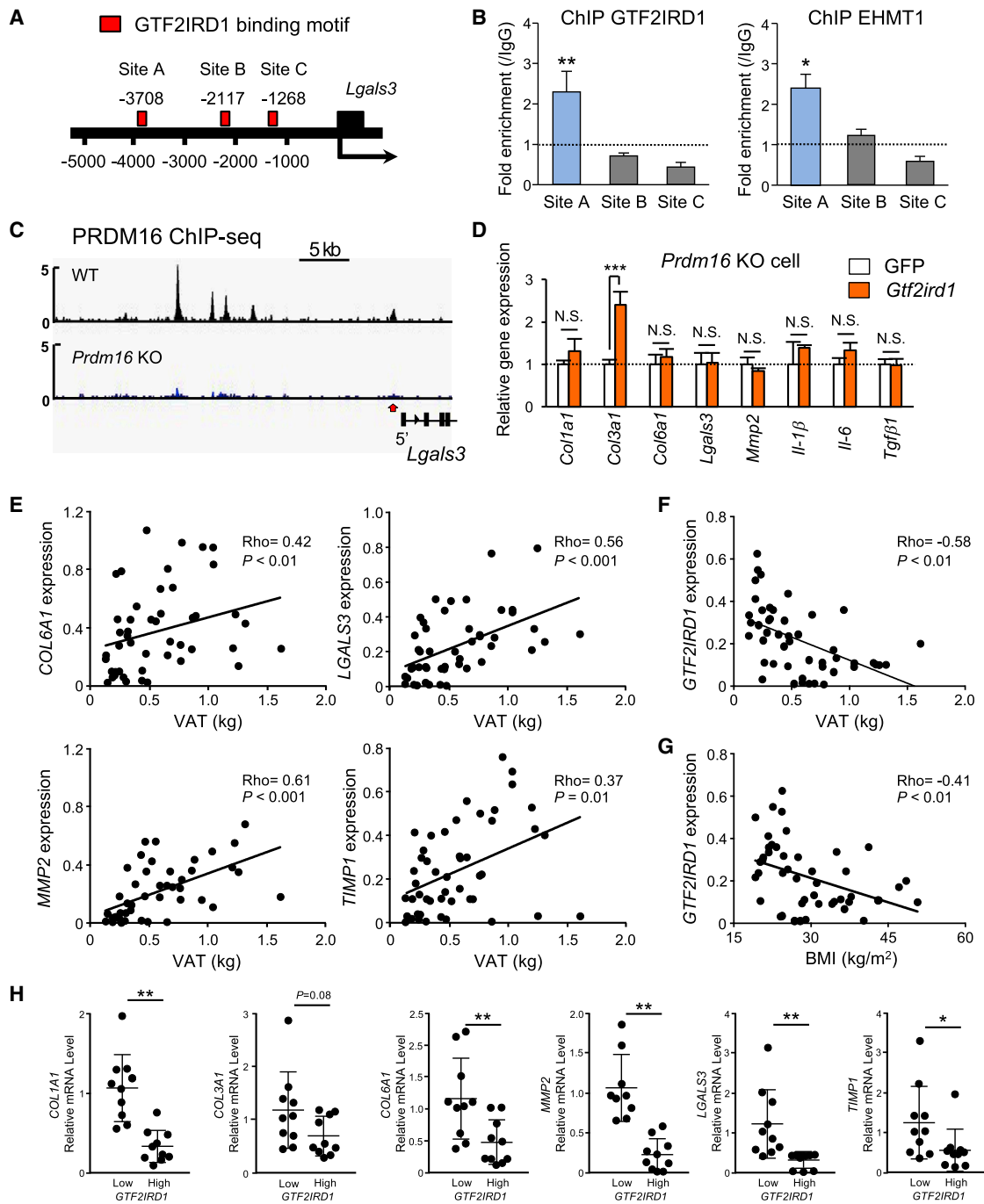


Figure 5. Regulatory Mechanisms of Adipose Fibrosis by GTF2IRD1

(A) Location of GTF2IRD1 binding motifs at the promoter/enhancer regions of *Lgals3* (sites A–C).

(B) ChIP assays in brown adipocytes using specific antibodies against GTF2IRD1 and EHMT1. Fold enrichment at each GTF2IRD1 binding motif site in (A) was assessed by qPCR compared with IgG control. n = 3. *p < 0.05, **p < 0.01.

(C) Enrichment of PRDM16 on the *Lgals3* gene in BAT of wild-type and *Prdm16*^{-/-} (knockout [KO]) mice. The dataset was obtained from the dataset in (Harms et al., 2015).

(D) Relative mRNA expression of pro-fibrosis and pro-inflammatory genes in *Prdm16* KO adipocytes expressing GFP or GTF2IRD1. Cells were treated with TGF- β to induce fibrosis. ***p < 0.001, n = 4. Data in (B) and (D) are represented as mean \pm SEM. N.S., not significant.

(E) Relative mRNA levels of pro-fibrotic genes in the abdominal subcutaneous WAT of adult human subjects (ages 25–65 years) drawn from the UCSF IDEO cohort. n = 48. To ensure an ethnically mixed population of lean and obese people, the random sample included 22 Caucasian (12 obese and 10 lean) and 26 Chinese (15 obese and 11 lean) subjects. Visceral adipose tissue (VAT) mass was measured by DEXA.

(legend continued on next page)

GTF2IRD1-Mediated Inhibition of Adipose Tissue Fibrosis Improves Systemic Glucose Homeostasis Independent of Body-Weight

Given that adipose tissue fibrosis has been associated with increased type 2 diabetes risk, our results motivated us to investigate the potential impact of reduced adipose fibrosis in the context of increased GTF2IRD1 expression on systemic glucose tolerance and insulin sensitivity *in vivo*. With this in mind, *Gtf2ird1* Tg mice and littermate controls were fed either a RD or a HFD for up to 16 weeks. *Gtf2ird1* Tg mice gained slightly less weight than controls after consuming an HFD for 15 weeks, with this phenotype persisting thereafter (Figures 6A, S6A, and S6B). Consistent with this modest reduction in body-weight gain, *Gtf2ird1* Tg mice on a HFD trended toward slightly higher whole-body energy expenditure (VO_2) compared with controls upon cold exposure, with no difference seen in food intake or locomotor activity (Figures S6C–S6E).

Notwithstanding, *Gtf2ird1* Tg mice exhibited a robust improvement in systemic glucose tolerance relative to controls when assessed after the mice consumed a HFD for 10 weeks. This improved glucose tolerance was evident before any differences in body-weight and fat mass had emerged between the two groups (Figures 6B and S6A). Fasting blood glucose levels were also significantly lower in *Gtf2ird1* Tg mice than in controls. Moreover, insulin tolerance was significantly better in *Gtf2ird1* Tg mice than in controls after 10 weeks on a HFD (Figure 6C), and *Gtf2ird1* Tg mice had reduced fasting serum insulin levels when measured at 12 weeks of HFD (Figure 6D). Importantly, inhibition of adipose tissue fibrosis was seen in the *Gtf2ird1* Tg mice in conjunction with the improved systemic glucose homeostasis; at 11 weeks of HFD many of the pro-fibrosis genes were significantly reduced in the inguinal WAT and the BAT of *Gtf2ird1* Tg mice relative to controls (Figure 6E, also see Figures 3C and 3D). In contrast, no significant change was found in the expression of pro-inflammatory genes between the two groups (Figure 6F). These results indicate that repression of adipose tissue fibrosis, rather than repression of adipose tissue inflammation, was tightly associated with an improvement in systemic glucose metabolism.

Because BAT thermogenesis in mice is active under ambient temperature at 22°C, we asked whether the ability of GTF2IRD1 to improve systemic glucose homeostasis would be diminished in the absence of thermal stress. We thus examined *Gtf2ird1* Tg and control mice that were fed a HFD at thermoneutrality (30°C). Although this abolished any differences in body-weight gain (Figure 6G), and whole-body energy expenditure (Figure S6C) between the genotypes, *Gtf2ird1* Tg mice living at thermoneutrality still had better glucose tolerance compared with the littermate controls after 10 weeks of HFD (Figure 6H). Consistent with the observations, the hydroxyproline assay found significantly less adipose tissue fibrosis in the BAT and the inguinal WAT of *Gtf2ird1* Tg, but not in the epididymal WAT, than controls at 10 weeks of HFD, even at 30°C (Figures 6I and S6F). No difference was found in the expression of pro-inflammatory genes

and thermogenic genes between the two groups (Figure S6G). Under a RD condition, no difference was observed in adipose tissue fibrosis and systemic glucose tolerance between the genotypes (Figure S7). These data suggest repression of adipose tissue fibrosis is a primary effect of GTF2IRD1 that alleviates diet-induced glucose tolerance and insulin resistance, even in the absence of thermal stress.

Repression of Adipose Tissue Fibrosis by GTF2IRD1 Improves Glucose Uptake and Insulin Sensitivity in BAT

To determine the tissues responsible for this improved glucose tolerance, we performed ^{18}F -fluoro-2-deoxy-D-glucose (^{18}F -FDG)-PET/CT scanning on *Gtf2ird1* Tg and control mice on a HFD. We found that *Gtf2ird1* Tg mice had significantly increased ^{18}F -FDG uptake in the iBAT, but not in the skeletal muscle (soleus) or the liver (Figures 7A and 7B). This increase in glucose uptake in BAT is partly through enhanced insulin sensitivity, because the BAT and the inguinal WAT from *Gtf2ird1* Tg mice under HFD showed significantly higher insulin signaling based on Akt phosphorylation, whereas no difference was found in insulin signaling of either the skeletal muscle or the liver (Figures 7C and 7D).

Accordingly, we asked whether GTF2IRD1 is required, cell-autonomously, for insulin-dependent glucose uptake by brown adipocytes. To this end, we measured insulin-stimulated 2-deoxy-D-glucose (2DG) uptake in differentiated brown adipocytes that were transduced with either scr (control) or with *Gtf2ird1* shRNA. We found that GTF2IRD1 deficiency significantly reduced insulin-dependent 2DG uptake relative to the control cells, a reduction that reached 71.4% when the cells were treated with TGF- β (Figure 7E). Conversely, GTF2IRD1 overexpression significantly increased insulin-dependent 2DG uptake by brown adipocytes and completely blocked the impact of TGF- β , which otherwise reduced insulin-stimulated 2DG uptake by 24% (Figure 7F). These results indicate that the mechanism by which GTF2IRD1 improves systemic glucose and insulin tolerance involves a tissue-specific enhancement of insulin sensitivity in BAT and inguinal WAT, at least in part, through blocking the inhibitory effect of TGF- β on adipose tissue fibrosis and insulin-responsive glucose uptake.

Collectively, our results point to the model illustrated in Figure 7G. In an obese state, TGF- β levels are increased in the adipose tissue and the circulation (Samad et al., 1997; Yadav et al., 2011), promoting adipose tissue fibrosis through the activation of Smad2/3 and the induction of pro-fibrotic genes, such as *Lgals3* and *Pcolce2*. GTF2IRD1 is a BAT-enriched transcription factor that is induced in the WAT by cold exposure through β 3-AR-dependent signaling and that, in turn, potentially inhibits TGF- β target pro-fibrosis genes by recruiting the PRDM16-EHMT1 complexes to their promoter/enhancer regions. Inhibition of adipocyte fibrosis by the PRDM16-GTF2IRD1 complex exerts a cell-autonomous effect that improves systemic glucose homeostasis independent of UCP1-mediated thermogenesis and body-weight loss.

(F) Correlation between GTF2IRD1 mRNA levels in the subcutaneous WAT and VAT mass. $n = 48$.

(G) Correlation between GTF2IRD1 mRNA levels in the subcutaneous WAT and BMI.

(H) Relative mRNA levels of indicated pro-fibrotic genes comparing the groups drawn from individuals with the lowest and highest expression of GTF2IRD1 in the subcutaneous WAT. * $p < 0.05$, ** $p < 0.01$. $n = 10$ per group. Data are presented as means \pm SD.

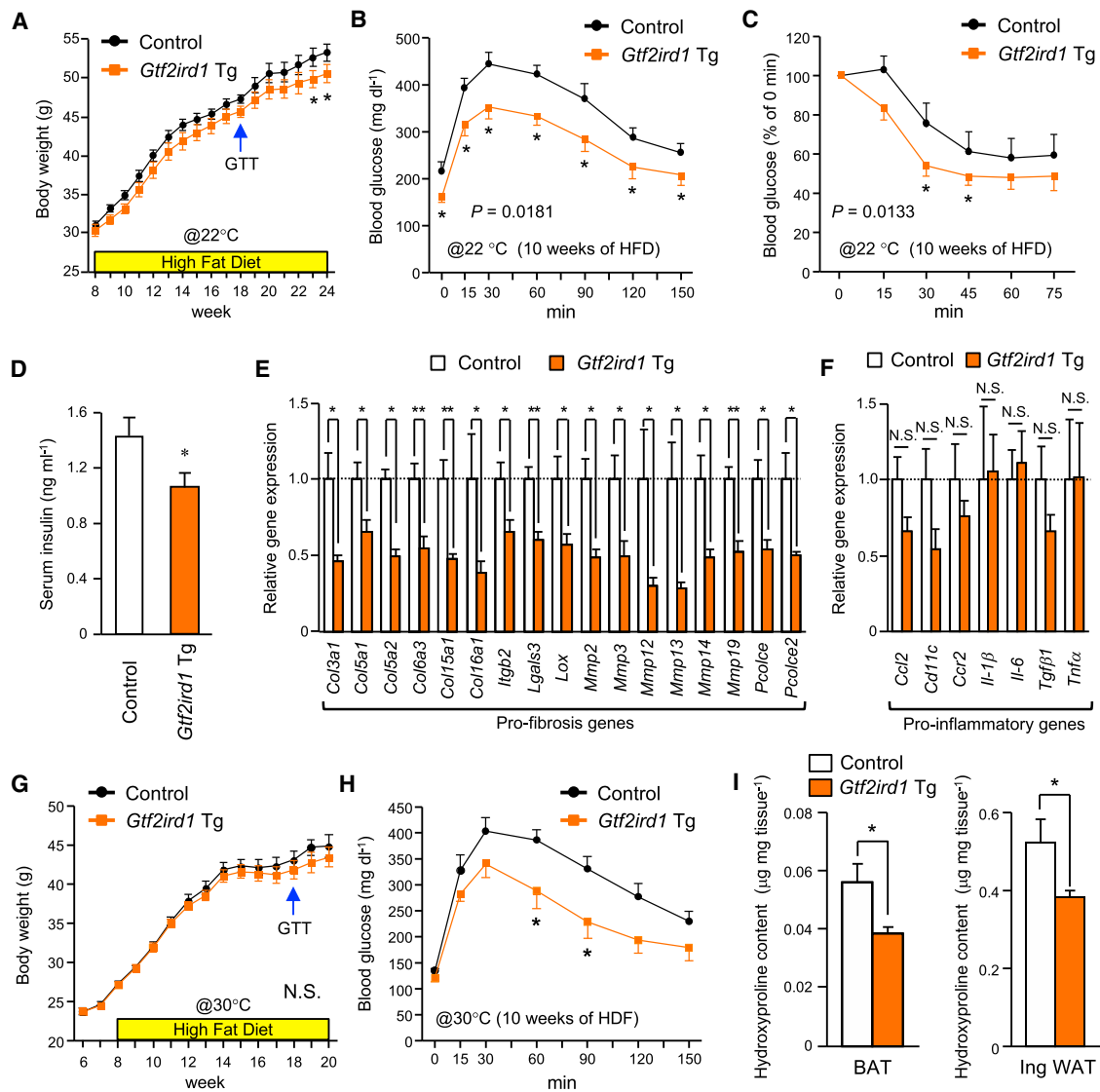


Figure 6. GTF2IRD1-Mediated Repression of Adipose Fibrosis Is Associated with Improved Systemic Glucose Homeostasis Independent of Body Weight

(A) Body-weight gain of *Gtf2ird1* Tg mice and the littermate controls (control) on a HFD at 22°C. n = 15. *p < 0.05.

(B) GTT in *Gtf2ird1* Tg mice and controls after 10 weeks of HFD at 22°C. *p < 0.05. n = 6–7.

(C) ITT in *Gtf2ird1* Tg mice and controls after 10 weeks of HFD at 22°C. *p < 0.05. n = 6–7.

(D) Serum concentrations of fasting insulin in *Gtf2ird1* Tg mice and controls after 11 weeks of HFD. *p < 0.05. n = 6–8.

(E) Relative mRNA expression of pro-fibrosis genes in the inguinal WAT of *Gtf2ird1* Tg mice and controls after 11 weeks of HFD. n = 6. *p < 0.05, **p < 0.01.

(F) Relative mRNA expression of pro-inflammatory genes in the inguinal WAT of *Gtf2ird1* Tg mice and controls after 11 weeks of HFD. N.S., not significant. n = 6.

(G) Body-weight gain of *Gtf2ird1* Tg mice and controls on a HFD under thermoneutrality (30°C). n = 9–15.

(H) GTT in *Gtf2ird1* Tg mice and controls after 10 weeks of HFD under thermoneutrality. *p < 0.05. n = 6–7.

(I) Hydroxyproline content in the BAT (left) and the inguinal WAT (right) from *Gtf2ird1* Tg mice and controls after 12 weeks of HFD under thermoneutrality. *p < 0.05. n = 6–7. All the data are presented as means ± SEM.

DISCUSSION

Due to its strong association with glucose intolerance and insulin resistance in humans, adipose tissue fibrosis is emerging as a signature of unhealthy adipose tissue (Sun et al., 2013b). On the other hand, active beige fat biogenesis is often associated with improvements in glucose homeostasis and insulin sensitivity (Chondronikola et al., 2014; Hanssen et al., 2015;

Sidossis and Kajimura, 2015). We demonstrate that the PRDM16 transcriptional complex not only activates brown/beige fat development, but also potently represses adipose tissue fibrosis through the direct interaction with GTF2IRD1. Notably, the time course analysis on a HFD found that reduced adipose tissue fibrosis by GTF2IRD1 improves systemic glucose homeostasis prior to changes in adipose tissue inflammation and body-weight loss. Furthermore, the transcriptional

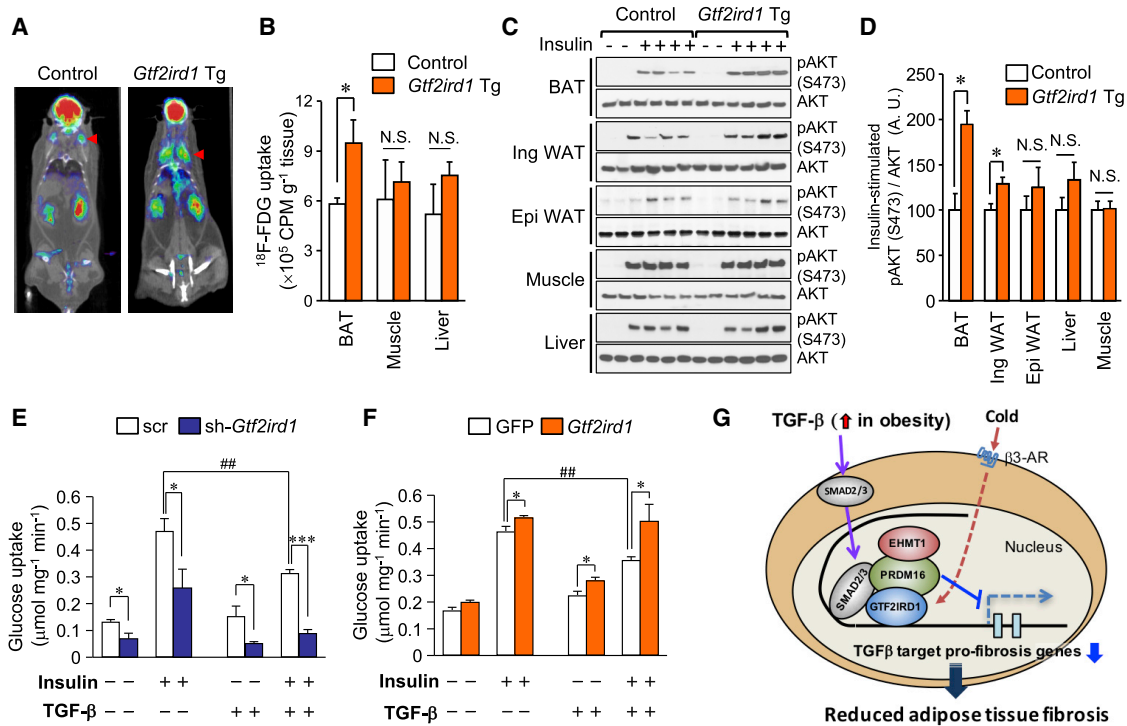


Figure 7. Repression of Adipose Tissue Fibrosis by GTF2IRD1 Improves BAT Glucose Uptake

(A) ^{18}F -Fluor-deoxyglucose (FDG) uptake was measured by ^{18}F FDG-PET/CT scan under ambient temperature. Representative images of control and *Gtf2ird1* Tg mice at 13 weeks of HFD are shown. Red arrowhead indicates interscapular BAT. $n = 5$.

(B) Quantification of ^{18}F -FDG uptake in the indicated organs in (A). * $p < 0.05$. N.S., not significant.

(C) Immunoblotting for phosphorylated (S473) and total AKT in the indicated tissues from *Gtf2ird1* Tg mice and the littermate controls. Mice were treated with saline or insulin before tissue harvest.

(D) Quantification of the insulin signaling assay in (C). $n = 4$. * $p < 0.05$. N.S., not significant.

(E) Glucose uptake in differentiated brown adipocytes expressing scrambled control (scr) or sh-*Gtf2ird1* (no. 2). Cells were treated with insulin (100 nM) and/or TGF- β (5 ng mL^{-1}). * $p < 0.05$, *** $p < 0.001$ between scrambled control and sh-*Gtf2ird1*. ## $p < 0.01$ between vehicle and TGF- β . $n = 6$.

(F) Glucose uptake in differentiated brown adipocytes expressing GFP or GTF2IRD1. Cells were treated with insulin (100 nM) and/or TGF- β (5 ng mL^{-1}). * $p < 0.05$ between GFP and *Gtf2ird1*. ## $p < 0.01$ between vehicle and TGF- β . $n = 6$. Data are presented as means \pm SEM.

(G) A proposed mechanism by which GTF2IRD1 controls adipose tissue fibrosis. See text for detail.

repression of pro-fibrosis genes by PRDM16 and GTF2IRD1 occurs independent of UCP1 expression. These results support the notion that improvement of systemic glucose homeostasis, when brown/beige fat biogenesis is activated, extends beyond UCP1-dependent energy dissipation (Kajimura et al., 2015). Although the conventional consensus has been that adipose tissue fibrosis is a consequence of obesity-induced chronic inflammation and hypoxia in the adipose tissue, the present study suggests that repression of adipose tissue fibrosis through the PRDM16-GTF2IRD1 pathway is sufficient to protect animals from diet-induced glucose tolerance and insulin resistance *in vivo*.

To better understand adipose tissue fibrosis, it is essential to identify primary sources of ECM proteins. In general, myofibroblasts, marked by α -smooth muscle actin, are considered a primary cell type that synthesizes and secretes ECM components (Wynn and Ramalingam, 2012); however, it is likely that multiple cell types contribute to ECM deposition in adipose tissues. For instance, perivascular cells expressing *Nestin* in the visceral WAT acquire pro-fibrotic characteristics and synthesize ECM proteins in response to platelet-derived

growth factor $R\alpha$ (PDGFR α) signaling (Iwayama et al., 2015). A recent study also demonstrated that PDGFR α -positive progenitors expressing high levels of CD9 drive adipose tissue fibrosis (Marcelin et al., 2017). On the other hand, a lineage tracing study showed that the majority of ECM-producing myofibroblasts in the dermal WAT originate from *Adiponectin*-expressing adipocytes through a process referred to as “adipocyte-myofibroblast transition” (Marangoni et al., 2015). In addition, inflammatory immune cells, including macrophages, appear to produce some ECM proteins (collagen I, fibronectin, and Tenascin-C) in obese WAT (Keophiphath et al., 2009). Of note, the cell-autonomous inhibitory action of GTF2IRD1 on pro-fibrosis genes is potent even when GTF2IRD1 is expressed in differentiated adipocytes; hence, the regulation of pro-fibrosis gene expression in mature adipocytes significantly contributes to ECM deposition in adipose tissues.

The mechanism of action of GTF2IRD1 is particularly intriguing because of its relevance in Williams-Beuren syndrome (OMIM194050). This rare genetic disease caused by a heterozygous deletion of ~ 1.5 Mb region at chromosome 7q11.23, a

region containing 26–28 genes, includes the *GTF2IRD1* gene (Makeyev et al., 2004; Tipney et al., 2004). Targeted deletion of *Gtf2rid1* in mice recapitulates some of the Williams-Beuren syndrome phenotypes, such as craniofacial abnormalities and diminished fear response (Enkhamdakh et al., 2009; Tassabehji et al., 2005; Young et al., 2008), although our fat-selective *Gtf2rid1* transgenic mice display no developmental defects in either craniofacial or overall body growth. Of particular relevance, there is an unusually high prevalence of glucose intolerance (up to 75%) among Williams-Beuren syndrome patients (Pober, 2010). Our data indicate that GTF2IRD1 is required for the cell-autonomous capacity to regulate fibrosis and glucose metabolism in adipocytes. Accordingly, future studies are warranted to determine the whole-body metabolic phenotype caused by the adipocyte-specific deletion of *Gtf2rid1*. Beyond genetic syndromes, it is also interesting to note that the expression of GTF2IRD1 is reciprocal to that of pro-fibrotic genes within the subcutaneous WAT of human subjects drawn from an ethnically diverse population. While visceral WAT depots are considered to be the site of major fibrotic tissue in mice, subcutaneous WAT fibrosis is epidemiologically linked to metabolic disease risk in adult humans (Divoux et al., 2010; Henegar et al., 2008; Lackey et al., 2014; Muir et al., 2016; Reggιο et al., 2016). In light of this study, our data in mice, which demonstrate that GTF2IRD1 represses diet-induced adipose tissue fibrosis in the BAT and the subcutaneous WAT thereby leading to an improvement in glucose tolerance, suggest a potentially important role for GTF2IRD1 in the regulation of glucose homeostasis in adult humans.

STAR★METHODS

Detailed methods are provided in the online version of this paper and include the following:

- KEY RESOURCES TABLE
- CONTACT FOR REAGENT AND RESOURCE SHARING
- EXPERIMENTAL MODEL AND SUBJECT DETAILS
 - Animals
 - Human Subjects
 - Cell Isolation Procedure
 - Culture Conditions
- METHOD DETAILS
 - Affinity Purification and Mass Spectrometry (MS)
 - Protein Interaction Analysis
 - Immunoblotting
 - Metabolic Studies
 - Micropet/CT Scan Analysis and ¹⁸F-FDG Uptake Analysis
 - *In Vivo* Insulin Stimulation Assay
 - Histological Analysis and Measurement of Fibrosis
 - RNA-Sequencing Analysis
 - Gene Expression Analysis
 - DNA Constructs and Viruses Production
 - *In Vitro* Glucose Uptake Assay
 - ChIP Assay
 - Macrophage Assay
- QUANTIFICATION AND STATISTICAL ANALYSIS
- DATA AND SOFTWARE AVAILABILITY

SUPPLEMENTAL INFORMATION

Supplemental Information includes seven figures and two tables and can be found with this article online at <https://doi.org/10.1016/j.cmet.2017.12.005>.

ACKNOWLEDGMENTS

We are grateful to Dr. C. Paillart for his assistance in the CLAMS studies, Dr. Y. Seo for his support in ¹⁸F-FDG-PET/CT studies, and Dr. P. Scherer at UT Southwestern Medical Center, Dr. P. Seale at the University of Pennsylvania, and Dr. L. Osborne and Dr. E. Tam at the University of Toronto for sharing materials. This work was supported by the NIH (DK97441 and DK108822 to S.K., DK103175 and DK098722 to S.K.K.), the UCSF Diabetes Research Center and Nutrition and Obesity Research Center P30 awards, and a training fellowship 5T32 DK007418 to D.L.A.) and by a cohort development grant by the UCSF Department of Medicine (to S.K.K.). Y.H. and K.I. were supported by the Manpei Suzuki Diabetes Foundation and the Uehara Memorial Foundation.

AUTHOR CONTRIBUTIONS

Conceptualization, Y.H. and S.K. Investigation, Y.H., K.I., Y.C., D.L.A., D.S., K.S., T.H., J.C., and S.K. Validation, P.M. and Y.Y. Data Curation, K.S. and P.C. Resources, D.L.A., K.S., S.K.K., and S.K. Writing & Editing, S.K.K. and S.K. Funding Acquisition, S.K.K. and S.K. Supervision, Y.I., P.C., S.K.K. and S.K.

Received: March 8, 2017

Revised: September 25, 2017

Accepted: December 5, 2017

Published: January 9, 2018

REFERENCES

- Aune, U.L., Ruiz, L., and Kajimura, S. (2013). Isolation and differentiation of stromal vascular cells to beige/brite cells. *J. Vis. Exp.* <https://doi.org/10.3791/50191>.
- Chimge, N.O., Makeyev, A.V., Ruddle, F.H., and Bayarsaihan, D. (2008). Identification of the TFII-I family target genes in the vertebrate genome. *Proc. Natl. Acad. Sci. USA* *105*, 9006–9010.
- Chondronikola, M., Volpi, E., Borsheim, E., Porter, C., Annamalai, P., Enerback, S., Lidell, M.E., Saraf, M.K., Labbe, S.M., Hurren, N.M., et al. (2014). Brown adipose tissue improves whole-body glucose homeostasis and insulin sensitivity in humans. *Diabetes* *63*, 4089–4099.
- Choy, L., and Derynck, R. (2003). Transforming growth factor-beta inhibits adipocyte differentiation by Smad3 interacting with CCAAT/enhancer-binding protein (C/EBP) and repressing C/EBP transactivation function. *J. Biol. Chem.* *278*, 9609–9619.
- Cohen, P., Levy, J.D., Zhang, Y., Frontini, A., Kolodin, D.P., Svensson, K.J., Lo, J.C., Zeng, X., Ye, L., Khandekar, M.J., et al. (2014). Ablation of PRDM16 and beige adipose causes metabolic dysfunction and a subcutaneous to visceral fat switch. *Cell* *156*, 304–316.
- Crewe, C., An, Y.A., and Scherer, P.E. (2017). The ominous triad of adipose tissue dysfunction: inflammation, fibrosis, and impaired angiogenesis. *J. Clin. Invest.* *127*, 74–82.
- Dankel, S.N., Svard, J., Mattha, S., Claussnitzer, M., Klötting, N., Glunk, V., Fandalyuk, Z., Grytten, E., Solsvik, M.H., Nielsen, H.J., et al. (2014). COL6A3 expression in adipocytes associates with insulin resistance and depends on PPARgamma and adipocyte size. *Obesity (Silver Spring)* *22*, 1807–1813.
- Divoux, A., Tordjman, J., Lacasa, D., Veyrie, N., Hugol, D., Aissat, A., Basdevant, A., Guerre-Millo, M., Poitou, C., Zucker, J.D., et al. (2010). Fibrosis in human adipose tissue: composition, distribution, and link with lipid metabolism and fat mass loss. *Diabetes* *59*, 2817–2825.
- Elias, J.E., and Gygi, S.P. (2007). Target-decoy search strategy for increased confidence in large-scale protein identifications by mass spectrometry. *Nat. Methods* *4*, 207–214.

- Enkhmandakh, B., Makeyev, A.V., Erdenechimeg, L., Ruddle, F.H., Chimge, N.O., Tussie-Luna, M.I., Roy, A.L., and Bayarsaihan, D. (2009). Essential functions of the Williams-Beuren syndrome-associated TFII-I genes in embryonic development. *Proc. Natl. Acad. Sci. USA* *106*, 181–186.
- Fournier, B., Murray, B., Gutzwiller, S., Marceletti, S., Marcellin, D., Bergling, S., Brachat, S., Persohn, E., Pierrel, E., Bombard, F., et al. (2012). Blockade of the activin receptor IIb activates functional brown adipogenesis and thermogenesis by inducing mitochondrial oxidative metabolism. *Mol. Cell. Biol.* *32*, 2871–2879.
- Halberg, N., Khan, T., Trujillo, M.E., Wernstedt-Asterholm, I., Attie, A.D., Sherwani, S., Wang, Z.V., Landskroner-Eiger, S., Dineen, S., Magalang, U.J., et al. (2009). Hypoxia-inducible factor 1alpha induces fibrosis and insulin resistance in white adipose tissue. *Mol. Cell. Biol.* *29*, 4467–4483.
- Hanssen, M.J., Hoeks, J., Brans, B., van der Lans, A.A., Schaart, G., van den Driessche, J.J., Jorgensen, J.A., Boekschoten, M.V., Hesselink, M.K., Havekes, B., et al. (2015). Short-term cold acclimation improves insulin sensitivity in patients with type 2 diabetes mellitus. *Nat. Med.* *21*, 863–865.
- Harms, M.J., Ishibashi, J., Wang, W., Lim, H.W., Goyama, S., Sato, T., Kurokawa, M., Won, K.J., and Seale, P. (2014). Prdm16 is required for the maintenance of brown adipocyte identity and function in adult mice. *Cell Metab.* *19*, 593–604.
- Harms, M.J., Lim, H.W., Ho, Y., Shapira, S.N., Ishibashi, J., Rajakumari, S., Steger, D.J., Lazar, M.A., Won, K.J., and Seale, P. (2015). PRDM16 binds MED1 and controls chromatin architecture to determine a brown fat transcriptional program. *Genes Dev.* *29*, 298–307.
- Henegar, C., Tordjman, J., Achard, V., Lacasa, D., Cremer, I., Guerre-Millo, M., Poitou, C., Basdevant, A., Stich, V., Viguier, N., et al. (2008). Adipose tissue transcriptomic signature highlights the pathological relevance of extracellular matrix in human obesity. *Genome Biol.* *9*, R14.
- Hosogai, N., Fukuhara, A., Oshima, K., Miyata, Y., Tanaka, S., Segawa, K., Furukawa, S., Tochino, Y., Komuro, R., Matsuda, M., et al. (2007). Adipose tissue hypoxia in obesity and its impact on adipocytokine dysregulation. *Diabetes* *56*, 901–911.
- Ikeda, K., Kang, Q., Yoneshiro, T., Camporez, J.P., Maki, H., Homma, M., Shinoda, K., Lu, X., Chen, Y., Maretich, P., et al. (2017). UCP1-independent signaling involving SERCA2b-mediated calcium cycling regulates beige fat thermogenesis and systemic glucose homeostasis. *Nat. Med.* <https://doi.org/10.1038/nm.4429>.
- Inagaki, T., Sakai, J., and Kajimura, S. (2016). Transcriptional and epigenetic control of brown and beige adipose cell fate and function. *Nat. Rev. Mol. Cell Biol.* *17*, 480–495.
- Iwayama, T., Steele, C., Yao, L., Dozmorov, M.G., Karamichos, D., Wren, J.D., and Olson, L.E. (2015). PDGFRalpha signaling drives adipose tissue fibrosis by targeting progenitor cell plasticity. *Genes Dev.* *29*, 1106–1119.
- Kajimura, S., Seale, P., Kubota, K., Lunsford, E., Frangioni, J.V., Gygi, S.P., and Spiegelman, B.M. (2009). Initiation of myoblast to brown fat switch by a PRDM16-C/EBP-beta transcriptional complex. *Nature* *460*, 1154–1158.
- Kajimura, S., Seale, P., and Spiegelman, B.M. (2010). Transcriptional control of brown fat development. *Cell Metab.* *11*, 257–262.
- Kajimura, S., Seale, P., Tomaru, T., Erdjument-Bromage, H., Cooper, M.P., Ruas, J.L., Chin, S., Tempst, P., Lazar, M.A., and Spiegelman, B.M. (2008). Regulation of the brown and white fat gene programs through a PRDM16/CtBP transcriptional complex. *Genes Dev.* *22*, 1397–1409.
- Kajimura, S., Spiegelman, B.M., and Seale, P. (2015). Brown and beige fat: physiological roles beyond heat generation. *Cell Metab.* *22*, 546–559.
- Keophiphath, M., Achard, V., Henegar, C., Rouault, C., Clement, K., and Lacasa, D. (2009). Macrophage-secreted factors promote a profibrotic phenotype in human preadipocytes. *Mol. Endocrinol.* *23*, 11–24.
- Kersey, P.J., Duarte, J., Williams, A., Karavidopoulou, Y., Birney, E., and Apweiler, R. (2004). The International Protein Index: an integrated database for proteomics experiments. *Proteomics* *4*, 1985–1988.
- Khan, T., Muise, E.S., Iyengar, P., Wang, Z.V., Chandalia, M., Abate, N., Zhang, B.B., Bonaldo, P., Chua, S., and Scherer, P.E. (2009). Metabolic dysregulation and adipose tissue fibrosis: role of collagen VI. *Mol. Cell. Biol.* *29*, 1575–1591.
- Koliwad, S.K., Streeper, R.S., Monetti, M., Cornelissen, I., Chan, L., Terayama, K., Naylor, S., Rao, M., Hubbard, B., and Farese, R.V., Jr. (2010). DGAT1-dependent triacylglycerol storage by macrophages protects mice from diet-induced insulin resistance and inflammation. *J. Clin. Invest.* *120*, 756–767.
- Koncarevic, A., Kajimura, S., Cornwall-Brady, M., Andreucci, A., Pullen, A., Davies, M., Sako, D., Liu, J., Kumar, R., Burton, R., et al. (2012). A novel therapeutic approach to treating obesity through modulation of TGFβ signaling. *Endocrinology* *153*, 3133–3146.
- Kramer, A., Green, J., Pollard, J., Jr., and Tugendreich, S. (2014). Causal analysis approaches in ingenuity pathway analysis. *Bioinformatics* *30*, 523–530.
- Lackey, D.E., Burk, D.H., Ali, M.R., Mostaedi, R., Smith, W.H., Park, J., Scherer, P.E., Seay, S.A., McCoin, C.S., Bonaldo, P., et al. (2014). Contributions of adipose tissue architectural and tensile properties toward defining healthy and unhealthy obesity. *Am. J. Physiol. Endocrinol. Metab.* *306*, E233–E246.
- Lee, K.Y., Russell, S.J., Ussar, S., Boucher, J., Vernochet, C., Mori, M.A., Smyth, G., Rourk, M., Cederquist, C., Rosen, E.D., et al. (2013). Lessons on conditional gene targeting in mouse adipose tissue. *Diabetes* *62*, 864–874.
- Makeyev, A.V., Erdenechimeg, L., Mungunsukh, O., Roth, J.J., Enkhmandakh, B., Ruddle, F.H., and Bayarsaihan, D. (2004). GTF2IRD2 is located in the Williams-Beuren syndrome critical region 7q11.23 and encodes a protein with two TFII-I-like helix-loop-helix repeats. *Proc. Natl. Acad. Sci. USA* *101*, 11052–11057.
- Marangoni, R.G., Korman, B.D., Wei, J., Wood, T.A., Graham, L.V., Whitfield, M.L., Scherer, P.E., Tourtellotte, W.G., and Varga, J. (2015). Myofibroblasts in murine cutaneous fibrosis originate from adiponectin-positive intradermal progenitors. *Arthritis Rheumatol.* *67*, 1062–1073.
- Marcelin, G., Ferreira, A., Liu, Y., Atlan, M., Aron-Wisnewsky, J., Pelloux, V., Botbol, Y., Ambrosini, M., Fradet, M., Rouault, C., et al. (2017). A PDGFRalpha-mediated switch toward CD9high adipocyte progenitors controls obesity-induced adipose tissue fibrosis. *Cell Metab.* *25*, 673–685.
- Martinez-Martinez, E., Calvier, L., Rossignol, P., Rousseau, E., Fernandez-Celis, A., Jurado-Lopez, R., Laville, M., Cachofeiro, V., and Lopez-Andres, N. (2016). Galectin-3 inhibition prevents adipose tissue remodeling in obesity. *Int. J. Obes. (Lond.)* *40*, 1034–1038.
- McDonald, M.E., Li, C., Bian, H., Smith, B.D., Layne, M.D., and Farmer, S.R. (2015). Myocardin-related transcription factor a regulates conversion of progenitors to beige adipocytes. *Cell* *160*, 105–118.
- Meng, X.M., Nikolic-Paterson, D.J., and Lan, H.Y. (2016). TGF-beta: the master regulator of fibrosis. *Nat. Rev. Nephrol.* *12*, 325–338.
- Muir, L.A., Neeley, C.K., Meyer, K.A., Baker, N.A., Brosius, A.M., Washabaugh, A.R., Varban, O.A., Finks, J.F., Zamarron, B.F., Flesher, C.G., et al. (2016). Adipose tissue fibrosis, hypertrophy, and hyperplasia: correlations with diabetes in human obesity. *Obesity (Silver Spring)* *24*, 597–605.
- Ohno, H., Shinoda, K., Ohyama, K., Sharp, L.Z., and Kajimura, S. (2013). EHMT1 controls brown adipose cell fate and thermogenesis through the PRDM16 complex. *Nature* *504*, 163–167.
- Park, J., and Scherer, P.E. (2012). Adipocyte-derived endotrophin promotes malignant tumor progression. *J. Clin. Invest.* *122*, 4243–4256.
- Pasarica, M., Gowronska-Kozak, B., Burk, D., Remedios, I., Hymel, D., Gimble, J., Ravussin, E., Bray, G.A., and Smith, S.R. (2009). Adipose tissue collagen VI in obesity. *J. Clin. Endocrinol. Metab.* *94*, 5155–5162.
- Pober, B.R. (2010). Williams-Beuren syndrome. *N. Engl. J. Med.* *362*, 239–252.
- Rausch, M.E., Weisberg, S., Vardhana, P., and Tortorello, D.V. (2008). Obesity in C57BL/6J mice is characterized by adipose tissue hypoxia and cytotoxic T-cell infiltration. *Int. J. Obes. (Lond.)* *32*, 451–463.
- Reggio, S., Rouault, C., Poitou, C., Bichet, J.C., Prifti, E., Bouillot, J.L., Rizkalla, S., Lacasa, D., Tordjman, J., and Clement, K. (2016). Increased basement membrane components in adipose tissue during obesity: links with TGFbeta and metabolic phenotypes. *J. Clin. Endocrinol. Metab.* *101*, 2578–2587.
- Samad, F., Yamamoto, K., Pandey, M., and Loskutoff, D.J. (1997). Elevated expression of transforming growth factor-beta in adipose tissue from obese mice. *Mol. Med.* *3*, 37–48.

- Seale, P., Conroe, H.M., Estall, J., Kajimura, S., Frontini, A., Ishibashi, J., Cohen, P., Cinti, S., and Spiegelman, B.M. (2011). Prdm16 determines the thermogenic program of subcutaneous white adipose tissue in mice. *J. Clin. Invest.* *121*, 96–105.
- Shinoda, K., Luijten, I.H., Hasegawa, Y., Hong, H., Sonne, S.B., Kim, M., Xue, R., Chondronikola, M., Cypess, A.M., Tseng, Y.H., et al. (2015). Genetic and functional characterization of clonally derived adult human brown adipocytes. *Nat. Med.* *21*, 389–394.
- Sidossis, L., and Kajimura, S. (2015). Brown and beige fat in humans: thermogenic adipocytes that control energy and glucose homeostasis. *J. Clin. Invest.* *125*, 478–486.
- Spencer, M., Yao-Borengasser, A., Unal, R., Rasouli, N., Gurley, C.M., Zhu, B., Peterson, C.A., and Kern, P.A. (2010). Adipose tissue macrophages in insulin-resistant subjects are associated with collagen VI and fibrosis and demonstrate alternative activation. *Am. J. Physiol. Endocrinol. Metab.* *299*, E1016–E1027.
- Sun, K., Halberg, N., Khan, M., Magalang, U.J., and Scherer, P.E. (2013a). Selective inhibition of hypoxia-inducible factor 1 α ameliorates adipose tissue dysfunction. *Mol. Cell. Biol.* *33*, 904–917.
- Sun, K., Park, J., Gupta, O.T., Holland, W.L., Auerbach, P., Zhang, N., Goncalves Marangoni, R., Nicoloso, S.M., Czech, M.P., Varga, J., et al. (2014). Endotrophin triggers adipose tissue fibrosis and metabolic dysfunction. *Nat. Commun.* *5*, 3485.
- Sun, K., Tordjman, J., Clement, K., and Scherer, P.E. (2013b). Fibrosis and adipose tissue dysfunction. *Cell Metab.* *18*, 470–477.
- Tassabehji, M., Hammond, P., Karmiloff-Smith, A., Thompson, P., Thorgeirsson, S.S., Durkin, M.E., Popescu, N.C., Hutton, T., Metcalfe, K., Rucka, A., et al. (2005). GTF2IRD1 in craniofacial development of humans and mice. *Science* *310*, 1184–1187.
- Thompson, P.D., Webb, M., Beckett, W., Hinsley, T., Jowitt, T., Sharrocks, A.D., and Tassabehji, M. (2007). GTF2IRD1 regulates transcription by binding an evolutionarily conserved DNA motif 'GUCE'. *FEBS Lett.* *581*, 1233–1242.
- Tipney, H.J., Hinsley, T.A., Brass, A., Metcalfe, K., Donnai, D., and Tassabehji, M. (2004). Isolation and characterisation of GTF2IRD2, a novel fusion gene and member of the TFII-I family of transcription factors, deleted in Williams-Beuren syndrome. *Eur. J. Hum. Genet.* *12*, 551–560.
- Tripathi, S., Pohl, M.O., Zhou, Y., Rodriguez-Frandsen, A., Wang, G., Stein, D.A., Moulton, H.M., DeJesus, P., Che, J., Mulder, L.C., et al. (2015). Meta- and orthogonal integration of influenza "OMICS" data defines a role for UBR4 in virus budding. *Cell Host Microbe* *18*, 723–735.
- Wynn, T.A., and Ramalingam, T.R. (2012). Mechanisms of fibrosis: therapeutic translation for fibrotic disease. *Nat. Med.* *18*, 1028–1040.
- Xue, Y., Petrovic, N., Cao, R., Larsson, O., Lim, S., Chen, S., Feldmann, H.M., Liang, Z., Zhu, Z., Nedergaard, J., et al. (2009). Hypoxia-independent angiogenesis in adipose tissues during cold acclimation. *Cell Metab.* *9*, 99–109.
- Yadav, H., Quijano, C., Kamaraju, A.K., Gavrilova, O., Malek, R., Chen, W., Zervas, P., Zhigang, D., Wright, E.C., Stuelten, C., et al. (2011). Protection from obesity and diabetes by blockade of TGF- β /Smad3 signaling. *Cell Metab.* *14*, 67–79.
- Ye, J., Gao, Z., Yin, J., and He, Q. (2007). Hypoxia is a potential risk factor for chronic inflammation and adiponectin reduction in adipose tissue of ob/ob and dietary obese mice. *Am. J. Physiol. Endocrinol. Metab.* *293*, E1118–E1128.
- Young, E.J., Lipina, T., Tam, E., Mandel, A., Clapcote, S.J., Bechard, A.R., Chambers, J., Mount, H.T., Fletcher, P.J., Roder, J.C., et al. (2008). Reduced fear and aggression and altered serotonin metabolism in Gtf2ird1-targeted mice. *Genes Brain Behav.* *7*, 224–234.

STAR★METHODS

KEY RESOURCES TABLE

REAGENT or RESOURCE	SOURCE	IDENTIFIER
Antibodies		
GTF2IRD1	abcam	Cat# ab51524; RRID: AB_880320
GTF2IRD1	Novus Biologies	Cat# NBP1-91973; RRID: AB_11006170
beta-Actin-Peroxidase	Sigma-Aldrich	Cat# A3854; RRID: AB_262011
Flag-HRP	Sigma-Aldrich	Cat# A8592; RRID: AB_439702
UCP1	abcam	Cat# ab10983; RRID: AB_2241462
Mouse IgG (H+L)	Jackson ImmunoResearch	Cat# 715-035-150; RRID: AB_2340770
Phospho-Akt (Ser473)	CST	Cat# 4060; RRID: AB_2315049
Akt (pan)	CST	Cat# 4691; RRID: AB_915783
Rabbit IgG (H+L) Secondary Antibody, HRP	Jackson ImmunoResearch	Cat# 711-035-152; RRID: AB_10015282
EHMT1	R&D	Cat# PP-B0422-00; RRID: AB_2097494
PPAR-gamma (H-100)	Santa Cruz	Cat# sc-7196; RRID: AB_654710
HA-HRP	Roche	Cat#11-867-423-001; RRID: AB_390918
Mouse Endotrophin	Sun et al., 2014	N/A
Bacterial and Virus Strains		
GTF2IRD1 Adenovirus	Vector Biolabs	Cat# ADV-260890
eGFP adenovirus	Vector Biolabs	Cat# 1060
Biological Samples		
Purified GST-fused PRDM16 fragments	Kajimura et al., 2008	N/A
Human tissue samples	This paper	N/A
Chemicals, Peptides, and Recombinant Proteins		
Flag peptide	Sigma-Aldrich	Cat# F3290
Human Recombinant TGF-beta	Corning	Cat# 354039
CL316,243	Sigma-Aldrich	Cat# C5976
Rosiglitazone	Fisher	Cat# 71740
Puromycin dihydrochloride	Santa Cruz	Cat# sc-108071B
Forskolin	Sigma-Aldrich	Cat# C6886
G418	Roche	Cat# 04-727-878001
Deoxy-D-glucose, 2-[1,2-3H (N)]-	PerkinElmer	Cat# NET328250UC
2,2,2, Tribromoethanol	Alfa Aesar	Cat# A18706-06
Oil red O	Sigma-Aldrich	Cat# O0625
Coomassie Brilliant Blue R-250	Bio-Rad	Cat# 1610400
Cytochalasin B	Sigma-Aldrich	Cat# C6762
¹⁸ F-FDG	University of California San Francisco (UCSF) Radiopharmaceutical Facility	https://radiology.ucsf.edu/
Recombinant human M-CSF	Peptotech	Cat# 300-25
Bovine Serum Albumin	Sigma-Aldrich	Cat# A8806
Lipopolysaccharides	Sigma-Aldrich	Cat# L4391
Stearic acid	Nu-Chek Prep, Inc	Cat# S1111
Palmitic acid	Sigma-Aldrich	Cat# P0500
IL-4	Sigma-Aldrich	Cat# I1020
Critical Commercial Assays		
Hydroxyproline Assay Kit	Quickzyme Bioscience	Cat# QZBHYPRO1
Agarose ChIP kit	Pierce	Ca# 26156
Rat/Mouse Insulin ELISA Kit	EMD Millipore	Cat# EZRMI-13K

(Continued on next page)

Continued

REAGENT or RESOURCE	SOURCE	IDENTIFIER
Thermo Scientific Triglycerides Reagent	Thermo Fischer scientific	Cat# TR22421
HR Series NEFA-HR(2) Color Reagent A	Wako Diagnostics	Cat# 999-34691
HR Series NEFA-HR(2) Solvent A	Wako Diagnostics	Cat# 995-34791
HR Series NEFA-HR(2) Color Reagent B	Wako Diagnostics	Cat# 991-34891
HR Series NEFA-HR(2) Solvent B	Wako Diagnostics	Cat# 993-35191
Mouse TNF- α ELISA kit	Fisher Scientific	Cat# 5017331
Mouse MCP-1 ELISA kit	Fisher Scientific	Cat# 501125204
Mouse IL-6 ELISA kit	Fisher Scientific	Cat# 5017209
Deposited Data		
GTF2IRD1 Tg RNA-seq dataset	This paper	ArrayExpress: E-MTAB-4163
<i>Prdm16</i> Tg x <i>Ucp1</i> ^{-/-} RNA-seq dataset	Ikeda et al., 2017	ArrayExpress: E-MTAB-4085
Primary brown and white adipocytes RNA-seq	Shinoda et al., 2015	ArrayExpress: E-MTAB-2624
Experimental Models: Cell Lines		
293T	ATCC	Cat# CRL-3216
<i>Prdm16</i> knockout brown adipocytes	Harms et al., 2015	N/A
<i>Ucp1</i> knockout brown adipocytes	Ikeda et al., 2017	N/A
Immortalized brown preadipocytes	Ohno et al., 2013 ; Shinoda et al., 2015	N/A
Immortalized inguinal preadipocytes	Ohno et al., 2013 ; Shinoda et al., 2015	N/A
Experimental Models: Organisms/Strains		
Mouse: <i>Gtf2ird1</i> Tg	This paper	N/A
Mouse: <i>Ucp1</i> ^{-/-} ; B6.129-Up1tm1Kz/J	The Jackson Laboratory	Cat# 003124
Mouse: <i>Fabp4</i> - <i>Prdm16</i> Tg	Seale et al., 2011	N/A
Mouse: <i>Fabp4</i> - <i>Prdm16</i> Tg x <i>Ucp1</i> ^{-/-}	Ikeda et al., 2017	N/A
Mouse: <i>Ehmt1</i> ^{flox/flox}	Ohno et al., 2013	N/A
Oligonucleotides		
A full list of Primers for fibrosis, see Table S2	This paper	N/A
Recombinant DNA		
pMSCV-puro-GFP	Ohno et al., 2013	N/A
pMSCV-Flag-Ehmt1 (Glp1)	Ohno et al., 2013	N/A
pSUPER-Retro-shscrambled	Ohno et al., 2013	N/A
pSUPER-Retro-shEhmt1-#1	Ohno et al., 2013	N/A
pcDNA3.1-Gtf2ird1	This paper	N/A
pSUPER-Retro-shGtf2ird1-#1-2	This paper	N/A
pMSCV-Flag-Gtf2ird1	This paper	N/A
Software and Algorithms		
TopHat version 2.0.8	https://doi.org/10.1038/nprot.2012.016	N/A
Cuffdiff 2.1.1	https://doi.org/10.1038/nprot.2012.016	N/A
Metascape pathway analysis	Tripathi et al., 2015	N/A
Ingenuity Pathways Analysis	QIAGEN Bioinformatics	N/A
Image J Java 1.6.0_24	NIH	N/A
GraphPad Prism 6	GraphPad Software	N/A
SPSS Statistics 23	IBM	N/A
Other		
High Fat Diet	Research Diets	Cat# D12492

CONTACT FOR REAGENT AND RESOURCE SHARING

Further information and requests for resources and reagents should be directed to and will be fulfilled by the Lead Contact, Shingo Kajimura (shingo.kajimura@ucsf.edu).

EXPERIMENTAL MODEL AND SUBJECT DETAILS

Animals

All animal experiments were performed according to procedures approved by the Institutional Animal Care and Use Committee for animal care and handling at the University of California, San Francisco (UCSF). The *Fabp4-prdm16* transgenic mouse was reported previously (Seale et al., 2011). *Fabp4-Prdm16* transgenic mice in wild-type background and *Ucp1*^{-/-} background were backcrossed to the B16 background for more than eight generations (Ikeda et al., 2017). To generate fat-selective *Gtf2ird* transgenic mice, the complete *Gtf2ird* cDNA transcript variant 5 (NM_001081465.1) was cloned under the *Fabp4* gene promoter/enhancer. FVB mouse oocytes were injected with this construct by the UCSF Core Facility. Male mice were either maintained on a standard rodent chow or a 60% high-fat diet (Research Diets) at the indicated temperature under a 12hr light-dark cycle. Adipocyte tissue-specific EHMT1 KO mice (*Ehmt1*^{flox/flox}) was described previously by Ohno et al. (2013). For acute cold-exposure studies, samples were obtained from 9–10 week-old male C57BL/6 mice housed at 6°C for 3 days using a rodent incubator (Power Scientific, Inc. RIS33SD). For chronic cold exposure, wild-type and *Ucp1*^{-/-} mice under 12 weeks of HFD were kept under ambient temperature or 16°C for 10 days. β 3 adrenergic receptor agonist CL-316,243 (Sigma) at 1 mg/kg was injected intraperitoneally into mice daily for 7 days. No animals were excluded from the analyses.

Human Subjects

The study was approved by the UCSF Institutional Review Board. The study involved a random sample of 48 individuals (26 women, 22 men) aged 45 \pm 12 years (mean \pm SD), drawn from the UCSF Inflammation, Diabetes, Ethnicity and Obesity (IDEO) cohort, which includes subjects recruited from clinics at UCSF Medical Center and Zuckerberg San Francisco General Hospital. On initial enrollment, all IDEO cohort members sign consent forms including their willingness to participate in subsequent studies such as this one. To ensure an ethnically mixed population of lean and obese people, the random sample included 22 Caucasian (12 obese and 10 lean) and 26 Chinese (15 obese and 11 lean) subjects. No subjects were taking insulin, anti-inflammatory medications, glucocorticoids, or other medications likely to affect inflammation, including PPAR γ agonists; they had no history of heart failure, liver failure or renal dysfunction. The subjects covered a wide range of body mass index (BMI 18.5–52 kg/m²). Individuals were excluded for smoking, not being weight-stable for the last 3 months (change >3%), having any acute or chronic inflammatory or infectious disease, cancer, or alcohol consumption >20g per day.

Anthropometric and Body Composition Measurements

Height and weight were measured by standard procedures. Body composition was estimated by dual-energy X-ray absorptiometry (DEXA) using a Hologic Horizon/A scanner (3-minute whole body scan, <0.1 G mGy). Individuals, up to 450 lbs can be accurately measured by this device, and high-performance and "offset" scanning techniques were used to ensure complete coverage for those whose bodies were wider than the table width. Subsequent analyses used Hologic 12.4 software, following International Society for Clinical Densitometry guidelines, with precision error (1 SD) for total body fat and percent body fat of approximately 0.3 kg and 1%, respectively (calibration to correct for drifts using device-specific whole-body phantoms). Downstream analysis of these data are able to accurately estimate subcutaneous, visceral, gynoid, and android fat masses and percentages.

Subcutaneous WAT Sampling

Subcutaneous WAT samples were obtained from the subjects by 2 different methods: In most cases, samples were collected by aspirational needle biopsies using a 14–16 G needle from the peri-umbilical area under local anesthesia. A minority of samples were obtained prior to either elective bariatric or other abdominal surgery. WAT samples were freed of visible connective tissue and rinsed to remove blood and clots, after which they were further washed with Krebs-Ringer bicarbonate buffer supplemented with 1% BSA. The specimens were then immediately frozen in liquid nitrogen and stored at -80°C .

Cell Isolation Procedure

Primary brown and inguinal preadipocytes were obtained from male mice by collagenase digestion following the protocol that was published previously (Aune et al., 2013). Immortalized brown preadipocytes and inguinal white preadipocyte used in this study have been previously described (Ohno et al., 2013; Shinoda et al., 2015). *Prdm16* knockout brown adipocytes, a gift from Dr. Seale, were described previously (Harms et al., 2015). Bone marrow-derived macrophages (BMDMs) were isolated and differentiated as described previously (Koliwad et al., 2010). In brief, male mice euthanized with Avertin, and their tibias and femurs were flushed of bone marrow. The bone marrow cells were plated, and the myeloid precursors were differentiated for 6–8 days in RPMI 1640 (Gibco) containing 10% FBS (Atlanta Biologicals), penicillin/streptomycin, and recombinant M-CSF (for BMDMs; 10 ng/mL; Peprotech) to yield BMDMs.

Culture Conditions

Preadipocytes were differentiated by treating 90–95 % confluent cells in DMEM containing 10% FBS, 0.5 mM isobutylmethylxanthine, 125 nM indomethacin, 1 μM dexamethasone, 850 nM insulin, and 1 nM T3. Brown Adipocyte differentiation was induced by DMEM containing 10% FBS, 0.1 mM isobutylmethylxanthine, 25 nM indomethacin, 0.2 μM dexamethasone, 170 nM insulin, 0.2 nM T3. Two days after the induction, cells were switched to the maintenance medium containing 10% FBS, 850 nM insulin, 1 nM T3. TGF- β 1 (BD Bioscience) was added from the induction at indicated concentration. To stimulate respiration, immortalized brown fat preadipocytes were incubated with 10 μM forskolin for 4 h. All chemicals for cell culture were obtained

from Sigma unless otherwise indicated. After 5 days of differentiation, cells were washed with PBS and fixed with freshly prepared 4% formaldehyde for 15 min, and stained with Oil-Red-O solution for 20 min. Differentiated BMDMs were washed once with PBS and starved overnight, then treated for 24 hrs with 2% low-endotoxin Bovine Serum Albumin (Sigma A8806), 20 ng/mL IL-4, 200 ng/mL LPS (Sigma Aldrich L4391), or 500 μ M of either stearic acid or palmitic acid complexed to BSA in a 2:1 molar ratio.

METHOD DETAILS

Affinity Purification and Mass Spectrometry (MS)

Immortalized preadipocytes derived from mouse inguinal WAT were stably infected with retrovirus expressing FLAG-tagged PRDM16 or an empty vector. The adipocytes were grown to confluence and induced to differentiate under pro-adipogenic conditions containing 0.5 μ g/ml of rosiglitazone. Nuclear extracts from differentiated adipocytes were harvested for biochemical purification, as described in previous papers (Kajimura et al., 2008, 2009). The eluted complexes were TCA-precipitated, separated in a 4%–12% acrylamide gradient gel, and subsequently visualized by silver stain or coomassie blue dye. Gel-resolved proteins were excised, digested with trypsin, and individually analyzed by reverse-phase liquid chromatography with tandem mass spectrometry (LC-MS/MS) for peptide sequencing using a high-resolution hybrid mass spectrometer (LTQ-Orbitrap, Thermo Scientific) by employing the TOP10 method at the Taplin Biological Mass Spectrometry at Harvard Medical School. Data obtained from the LC-MS/MS was annotated using the IPI mouse database (Kersey et al., 2004). Proteins were considered significantly identified with at least two unique valid peptides, and the false discovery rate was estimated to be 0% using the target-decoy approach (Elias and Gygi, 2007).

Protein Interaction Analysis

Nuclear protein extracts were harvested from differentiated brown adipocytes expressing FLAG-PRDM16, FLAG-EHMT1, or an empty vector (control). Immunoprecipitation with FLAG-beads was carried out as previously described (Kajimura et al., 2008, 2009). Briefly, the nuclear extracts were incubated overnight at 4°C with Flag M2 agarose (SIGMA), washed, and eluted with a 3xFlag peptide. The eluted materials were analyzed by western blotting to detect endogenous GTF2IRD1 protein using the antibody against GTF2IRD1 (NBP1-91973, Novus). For in vitro binding assays, GST-fused PRDM16 fragments (1–223, 224–454, 455–680, 680–880, 881–1038 and 1039–1176) were described previously (Kajimura et al., 2008). ³⁵S-labeled proteins were made with a TNT reticulocyte lysate kit (Promega). Equal amounts of GST fusion proteins (2 μ g) were incubated overnight at 4°C with in vitro translated proteins in a binding buffer containing 20 mM HEPES (pH 7.7), 300 mM KCl, 2.5 mM MgCl₂, 0.05% NP40, 1 mM DTT, and 10% glycerol. The sepharose beads were then washed five times with the binding buffer. Bound proteins were separated by SDS-PAGE and analyzed by autoradiography. Total protein in the gel was visualized by coomassie blue dye.

Immunoblotting

Fully differentiated adipocytes were lysed in RIPA buffer containing 50 mM Tris, pH 7.5, 150 mM NaCl, 1% Triton-X, 10% glycerol, and cOmplete protease inhibitors (Roche). Total protein lysates were boiled with 4x NuPage LDS loading buffer (Invitrogen) that contained 100 mM DTT, loaded on a 4–15% SDS-PAGE, and subsequently transferred onto PVDF membranes. The PVDF membrane blots were blocked in 5% milk in Tris-buffered saline with Tween 20 (TBS-T) and incubated overnight with rabbit anti-GTF2IRD1 (NBP1-91973, Novus), rabbit anti-UCP-1 (ab10983, Abcam), anti-PPAR γ (H-100, Santa Cruz), anti-FLAG M2 (A8592, Sigma), anti-HA (Roche), or mouse anti- β -actin (A3854, Sigma) overnight. Anti-rabbit IgG (711-035-152, Jackson ImmunoResearch) was used as a secondary antibody for GTF2IRD1 and UCP1.

Metabolic Studies

Whole-body energy expenditure and associated metabolic parameters were performed using a temperature controlled Comprehensive Lab Animal Monitoring System (CLAMS) (Columbus Instruments). After mice were acclimatized to chambers under thermoneutrality (30°C), metabolic data were collected across different temperatures ranging from 30°C to 6°C. Serum level of insulin (Millipore), triglyceride (Thermo) and NEFA (Wako) were measured using commercially available kits. For glucose tolerance test experiments, male mice were fed a high-fat diet for 10 weeks. After 6 hours of fasting, the mice were injected intraperitoneally with glucose (1.2–1.5 g kg⁻¹). For insulin tolerance test experiments, male mice under a high-fat diet for 10 weeks were used. After 3 hours of fasting, the mice were injected intraperitoneally with insulin (0.6 U kg⁻¹).

Micropet/CT Scan Analysis and ¹⁸F-FDG Uptake Analysis

Mouse micro-PET/CT Scan was performed in wild-type and *Gtf2ird* Tg mice under ambient temperature following the established standard operating procedures that were approved by the UCSF Institutional Animal Care and Use Committee (IACUC) and Laboratory Animal Resource Center (LARC). Mice at 13 weeks of HFD were fasted for 5 h before each imaging session. A total of 100 μ Ci of ¹⁸F-FDG was administered via the tail vein, and PET scanning under 2% isoflurane anesthesia was started exactly at 55 minutes after FDG administration for 10 minutes, immediately followed by CT scanning. The data at a 10-minute time point were considered static and integrated for the data analysis. All mice were euthanized and dissected at 1 hour and 30 mins after injection. BAT, gastrocnemius muscle, and liver were collected and weighed. The radioactivity in the tissues was measured against known activity standards using a gamma-counter (Wizard 3; Perkin Elmer).

In Vivo Insulin Stimulation Assay

Mice kept under ambient temperature were anesthetized with Tribromoethanol (Avertin). 5U of human Insulin (Novo Noldisc) was injected into the inferior vena cavae. Livers (2min), BAT (4min) and soleus muscle (5min) were harvested after the injection and lysed in lysis buffer (50 mM Tris-HCl, pH 7.5, 150 mM NaCl, 10% (w/v) glycerol, 100 mM NaF, 10 mM EGTA, 1 mM Na₃VO₄, 1% (w/v) Triton X-100, 5 μM ZnCl₂, 2 mM), with protease inhibitor cocktail (cOmplete, Roche) and phosphatase inhibitor cocktail 2 and 3 (Sigma). The lysates were isolated and separated by SDS-polyacrylamide gel electrophoresis (SDS-PAGE). Akt (Pan) antibody (Cell Signaling) and Phospho-Akt (Ser473) antibody (Cell Signaling) were used for western blotting.

Histological Analysis and Measurement of Fibrosis

For histology, all tissues were placed in 10% paraformaldehyde for 24 hr, followed by 70% ethanol until processing. Tissues were processed, embedded in paraffin, sectioned at 5 μm, and stained with Hematoxylin & Eosin (H&E). To assess adipose fibrosis, Masson's trichrome, Picrosirius red staining and immunohistochemical staining with an anti-mouse endotrophin antibody (Park and Scherer, 2012; Sun et al., 2014) were performed. The endotrophin antibody was kindly provided by Dr. Philipp Scherer at UT South Western Medical Center. Images were acquired with a DM2000 digital camera (Leica). For the measurement of fibrosis, hydroxyproline content in adipose tissue was measured with a Hydroxyproline Assay Kit (Quickzyme Biosciences).

RNA-Sequencing Analysis

RNA-sequencing libraries were constructed from total RNA using Ovation RNA-sequencing system version 2 (NuGEN). The isolated RNA was reverse transcribed to cDNA using a combination of random hexameric and poly-T primers. The cDNA libraries were amplified using the Ultralow DR library kit (NuGEN) according to the manufacturer's instructions. Quality of the libraries was determined by Bioanalyzer (Agilent Technologies). Subsequently, high-throughput sequencing was performed using a HiSeq 2500 instrument (Illumina) at the UCSF Genomics Core Facility. Raw reads for each library were mapped using TopHat version 2.0.8 against the mouse (mm10) genome. The mapped reads were converted to FPKM (fragments per kilobase of exon per million fragments mapped) by running Cuffdiff 2.1.1 to determine gene expression. Bioinformatic analyses using the Metascape pathway analysis (Tripathi et al., 2015) and Ingenuity Pathways Analysis (Kramer et al., 2014) were carried out to find molecular functions and upstream signaling pathways that were significantly associated with differentially expressed genes by GTF2IRD1.

Gene Expression Analysis

Total RNA in mouse tissues was isolated using RiboZol reagents (AMRESCO) and reversed transcribed using an iScript cDNA synthesis kit (Bio-Rad). RNA isolation from intact and aspirated human subcutaneous WAT samples was done using the RNeasy Lipid Tissue Mini kit (Qiagen, Valencia, CA). Total RNA (1 μg) was reverse transcribed using the SensiFAST cDNA Synthesis Kit (Bioline Reagents Ltd, UK). Quantitative real-time PCR (qRT-PCR) was performed using Sybr Green (Applied Biosystems by Life Science, Warrington, UK). Each sample was run in duplicate, and the quantity of a particular gene in each sample was normalized to both beta-actin and Cyclophilin B for human samples and to TATA-binding protein, 36B4 or 18srRNA for mouse samples. Relative mRNA levels were determined by the $\Delta\Delta C_t$ method and expression normalized to an internal calibrator specific to each gene using the formula $2^{-\Delta\Delta C_t}$. For bone marrow-derived macrophages, relative mRNA abundance was normalized to the average of hypoxanthine quinine phosphoribosyl transferase and cyclophilin A. Primer sequences are provided in Table S2.

DNA Constructs and Viruses Production

The constructs were subcloned into a pMSCV-puro retroviral vector (Stratagene) or pcDNA3.1 (Invitrogen) using full-length Flag-tagged GTF2IRD1. For retrovirus production, Phoenix packaging cells were transfected at 70% confluence by calcium phosphate method with 10 μg of retroviral vectors. After 48 h, the viral supernatant was harvested and filtered. Cells were incubated overnight with the viral supernatant, supplemented with 8 μg/mL polybrene. Subsequently, puromycin (GFP and Flag-tagged GTF2IRD1), or G418 (shRNAs) were used for selection. The sequences used for retroviral shRNA expression vectors targeting GTF2IRD1 were described in Table S2. The retroviral shRNA expression vectors targeting EHMT1 were previously described (Ohno et al., 2013). The corresponding double-stranded DNA sequences were ligated into pSUPER-Retro (GFP-Neo) (Oligoengine) for retroviral expression. Adenovirus for mouse GTF2IRD1 were obtained from Vector Biolabs (SKU#: ADV-260890).

In Vitro Glucose Uptake Assay

Brown adipocytes were plated and differentiated in 12-well plates. Five days after inducing adipocyte differentiation, differentiated brown adipocytes were washed three times with PBS, and incubated in RPMI-1640 medium containing 1% BSA for 2 hr, and subsequently incubated in 1 mL/well PBS containing 100 nM insulin for 30 minutes at 37°C. After washing in PBS, the cells were incubated in 1 mL PBS containing 0.1 mM 2-deoxyglucose and 0.5 mCi/ml of 2 deoxy D [³H] glucose for 5 min. After washing in ice-cold PBS twice, the cells were solubilized in 0.4 mL of 2% SDS. ³H-glucose uptake was measured in scintillation cocktails using Beckman LS 3801 scintillation counter. Nonspecific deoxyglucose uptake was measured in the presence of cytochalasin B and subtracted from the total uptake.

ChIP Assay

Immortalized brown adipocytes were transduced with Flag-tagged GTF2IRD1 or GFP control. ChIP assays were performed following the manufacturer's instructions (Agarose ChIP kit; Pierce). Anti-GTF2IRD1 (NBP1-91973, Novus) and EHMT1 (R&D) were used to precipitate protein-bound DNA. Mouse IgG was used as a control. qRT-PCR analysis of recovered DNA fragments was performed using primers that span the putative GTF2IRD1-binding site A to C, respectively. qRT-PCR results were normalized to input values. Primer sequences used in the ChIP assays were provided in [Table S2](#).

Macrophage Assay

TNF- α , MCP-1 and IL6 concentrations secreted in the culture medium of isolated BMDMs were measured by ELISA kits (eBioscience) according to the manufacturer's instructions, and normalized to protein mass. mRNA expression of pro-inflammatory genes expressed by the BMDMs was measured by qRT-PCR.

QUANTIFICATION AND STATISTICAL ANALYSIS

Mouse data are presented as mean \pm SEM. Statistical significance was defined as $P < 0.05$ and determined by an unpaired Student's *t* test or one-way ANOVA throughout the study. Two-way ANOVA followed by post-hoc comparison was applied to determine the statistical difference in GTT and ITT. Human data are presented as means \pm SD, and all analyses were performed using features present in GraphPad Prism (version 7; GraphPad Software, Inc., San Diego, CA). The Shapiro-Wilks test was used to verify quantitative variables for normality distribution. Outliers were determined using the ROUT method with an average False Discovery Rate less than 1%. This process led to the exclusion of 4 outliers for final gene expression analysis. Mann-Whitney U test was used to compare differences between groups. Correlations between gene expression measurements and body composition parameters were assessed using Spearman's rank test. The statistical parameters and the number of mice used per experiment are found in the figure legends.

DATA AND SOFTWARE AVAILABILITY

RNA-sequencing reads are available in ArrayExpress (www.ebi.ac.uk) under accession number E-MTAB-4163. Bioinformatic software used in the study are publically available.

Cell Metabolism, Volume 27

Supplemental Information

Repression of Adipose Tissue Fibrosis

through a PRDM16-GTF2IRD1 Complex

Improves Systemic Glucose Homeostasis

Yutaka Hasegawa, Kenji Ikeda, Yong Chen, Diana L. Alba, Daniel Stifler, Kosaku Shinoda, Takashi Hosono, Pema Maretich, Yangyu Yang, Yasushi Ishigaki, Jingyi Chi, Paul Cohen, Suneil K. Koliwad, and Shingo Kajimura

Supplementary Figures

Repression of adipose tissue fibrosis through a PRDM16-GTF2IRD1 complex improves systemic glucose homeostasis.

Yutaka Hasegawa ^{1-3,6}, Kenji Ikeda ^{1-3,8}, Yong Chen ^{1-3,8}, Diana Alba ^{1,4,8}, Daniel Stifler ^{1,4}, Kosaku Shinoda ¹⁻³, Takashi Hosono ^{1-3,7}, Pema Maretich ¹⁻³, Yangyu Yang ¹⁻³, Yasushi Ishigaki ⁶, Jingyi Chi ⁵, Paul Cohen ⁵, Suneil Koliwad ^{1,4,*}, and Shingo Kajimura ^{1-3,*}

¹ UCSF Diabetes Center, CA, 94143

² Eli and Edythe Broad Center of Regeneration Medicine and Stem Cell Research, CA

³ Department of Cell and Tissue Biology, University of California, San Francisco, CA

⁴ Department of Medicine, University of California, San Francisco, CA

⁵ The Rockefeller University, Laboratory of Molecular Metabolism, NY

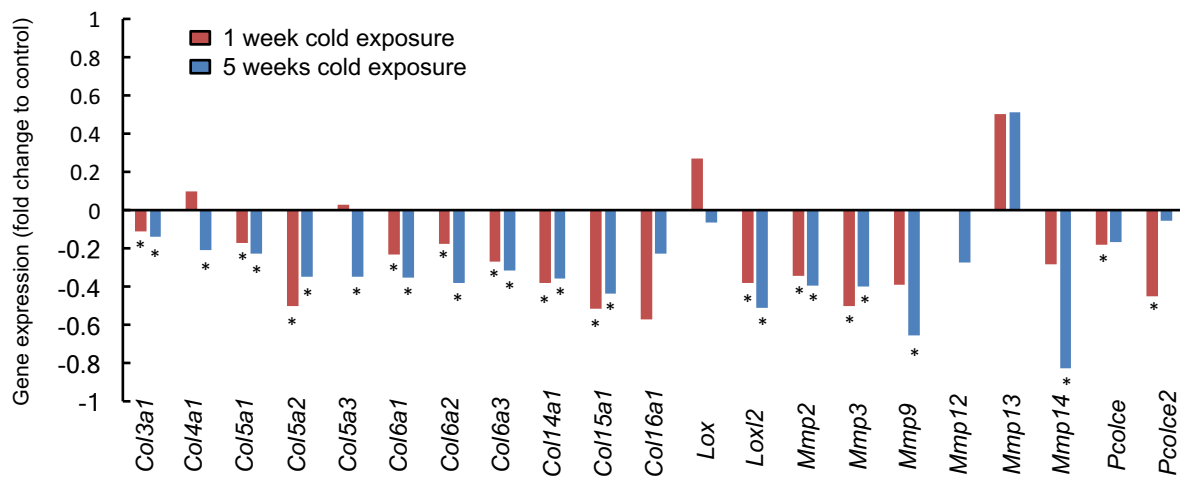
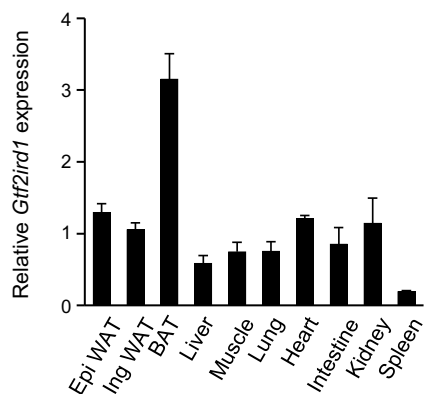
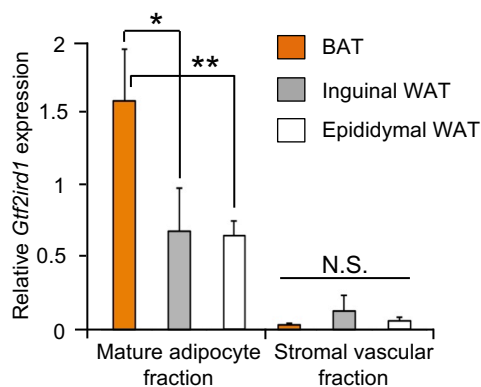
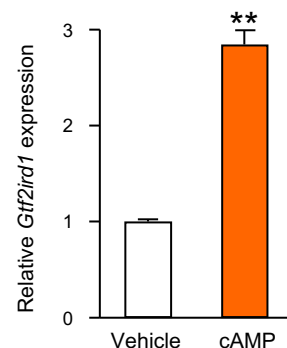
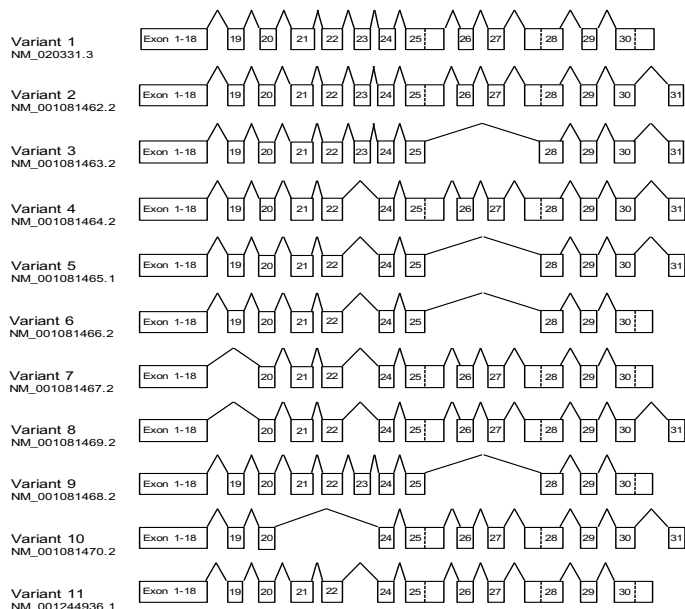
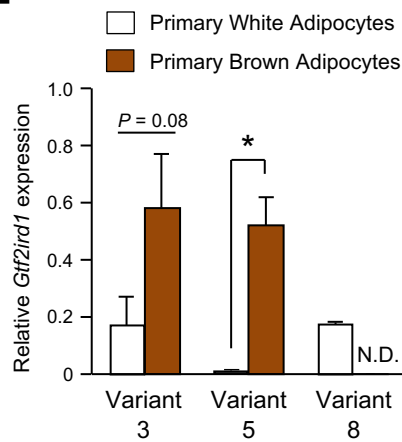
⁶ Division of Diabetes and Metabolism, Department of Internal Medicine, Iwate Medical University, Japan

⁷ Department of Chemistry and Life Science, College of Bioresource Sciences, Nihon University, Japan

⁸ Contributed equally

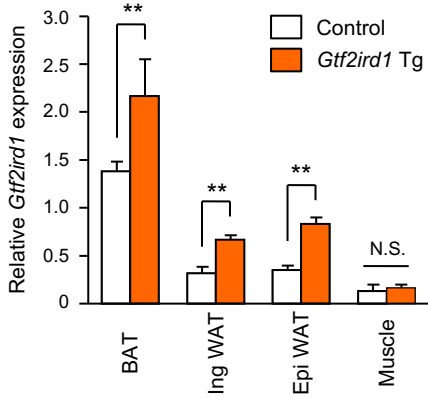
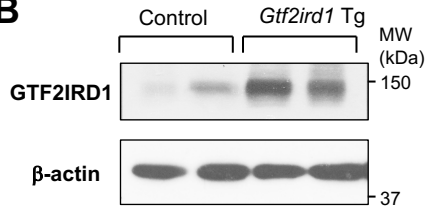
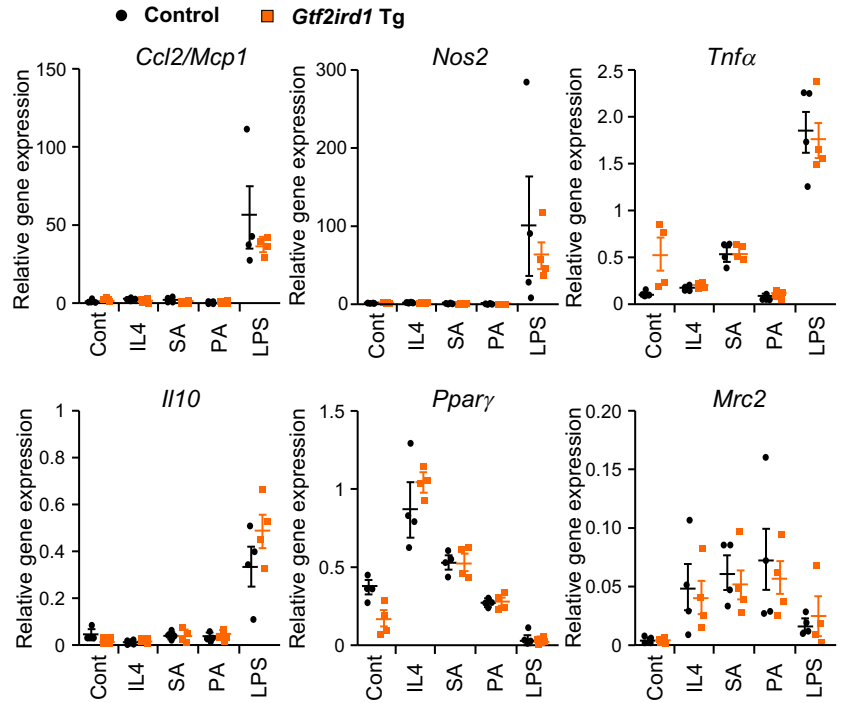
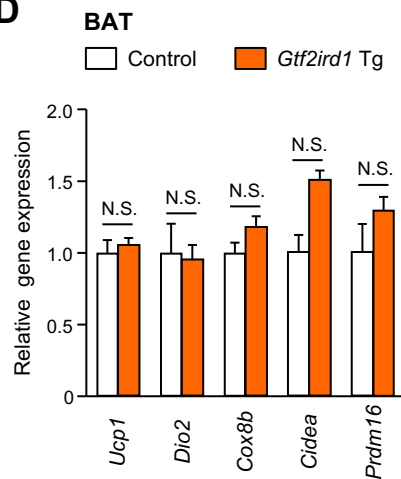
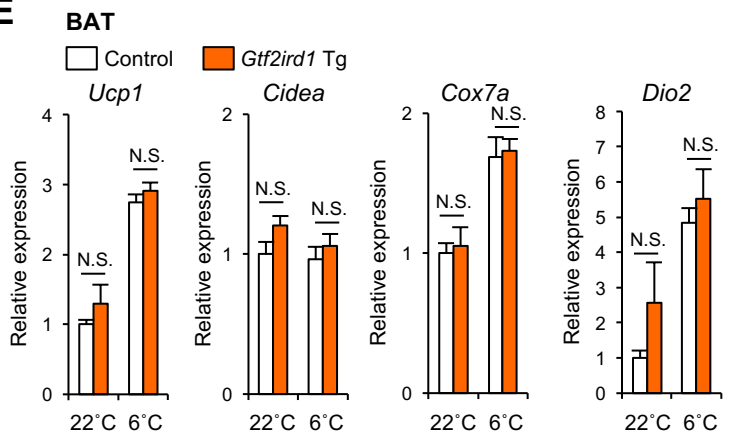
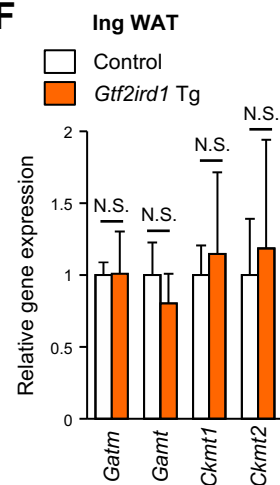
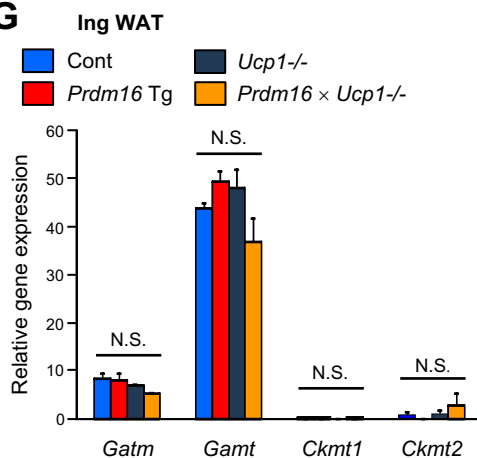
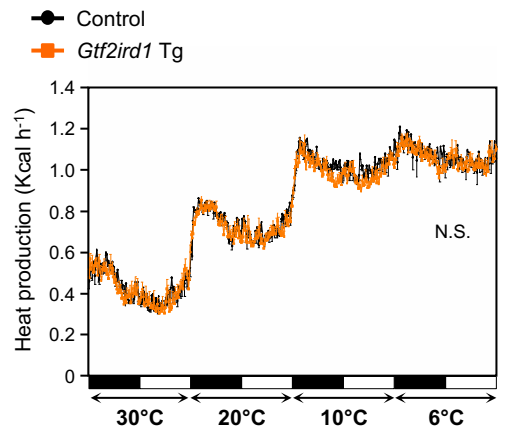
* Correspondence:

shingo.kajimura@ucsf.edu and Suneil.Koliwad2@ucsf.edu

A**B****C****D****E****F**

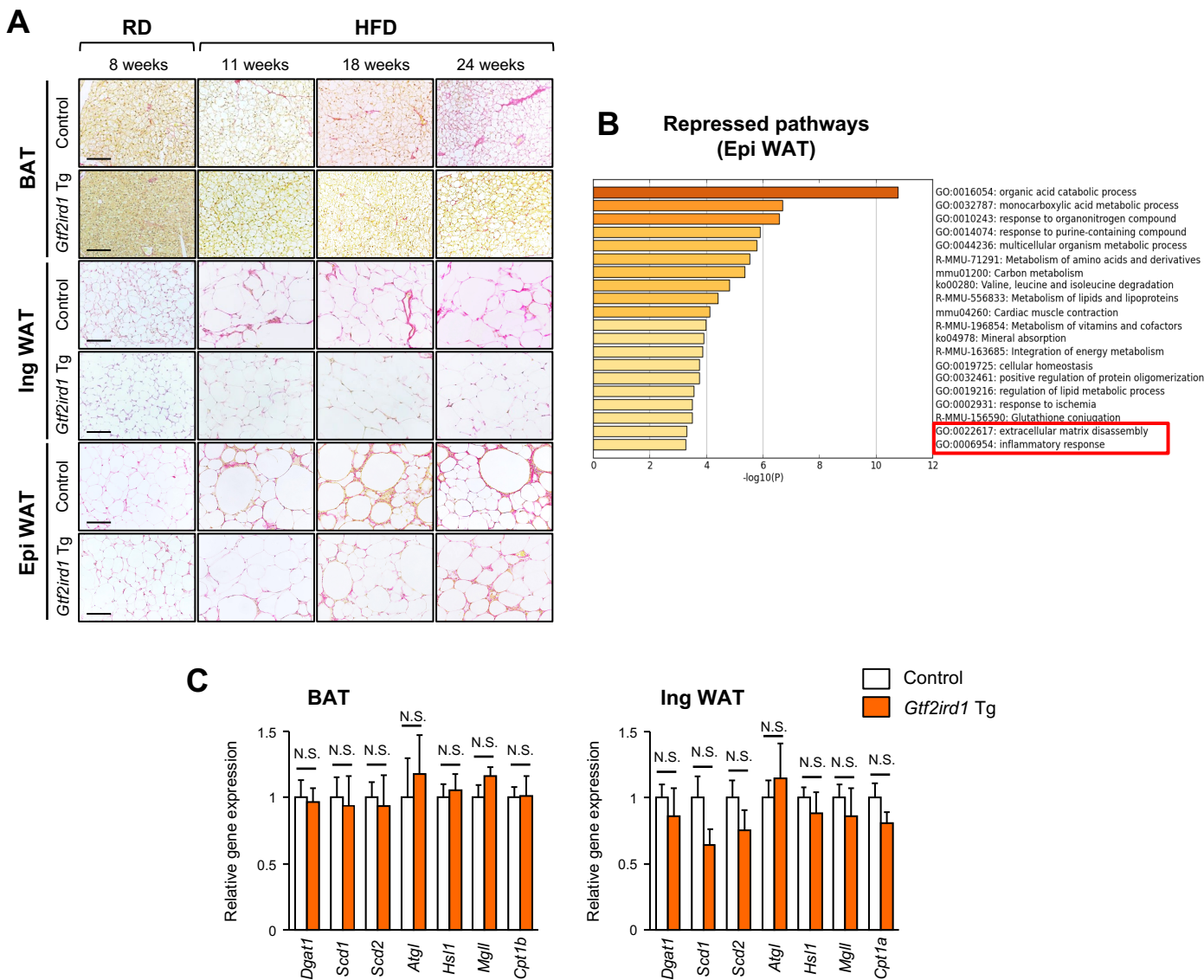
Supplementary Fig. 1 (related to Figure 1): Expression analyses of pro-fibrosis genes and *Gtf2ird1*.

- (A) Cold-induced changes in pro-fibrosis gene expression (fold change relative to ambient temperature) in the inguinal WAT from C57/Bl6 male mice. Mice were under ambient temperature or cold temperature at 4°C for 1 week (red) or 5 weeks (blue). The data were obtained from the microarray dataset published by Xue et al., (2009). * $P < 0.05$.
- (B) Tissue distribution of *Gtf2ird1* expression in indicated mouse tissues and organs. n=3-5.
- (C) Relative mRNA expression of *Gtf2ird1* in mature adipocytes and stromal vascular fractions from interscapular BAT, inguinal WAT, and epididymal WAT. * $P < 0.05$, ** $P < 0.01$, n=3. N.S., not significant.
- (D) Relative mRNA expression of *Gtf2ird1* in differentiated brown adipocytes treated with vehicle or forskolin (cAMP) at a dose of 10 μM for 4 hours. ** $P < 0.01$, n=3.
- (E) Eleven transcriptional variants of *Gtf2ird1* containing the indicated exons in mice. RNA-sequencing analysis detects variant 3, 5, and 8 in mouse interscapular BAT depots.
- (F) Relative mRNA expression of *Gtf2ird1* transcript variants in primary cultured differentiated white and brown adipocytes in mice. * $P < 0.05$, n=3. N.D., not detectable. Data shown in graphs are expressed as means \pm SEM.

A**B****C****D****E****F****G****H**

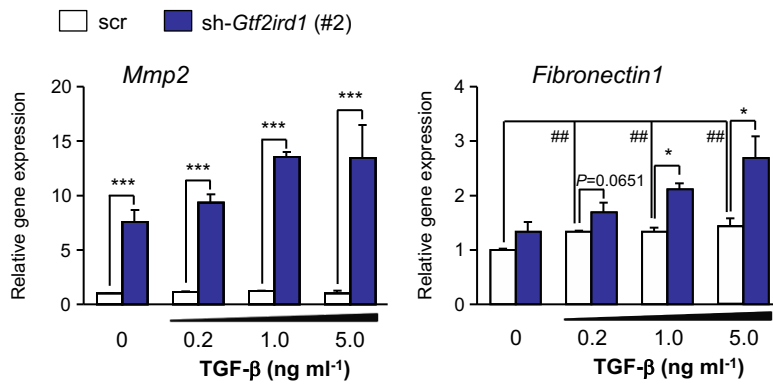
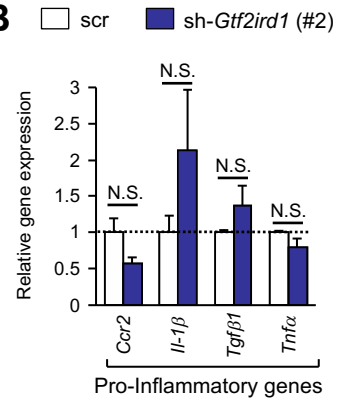
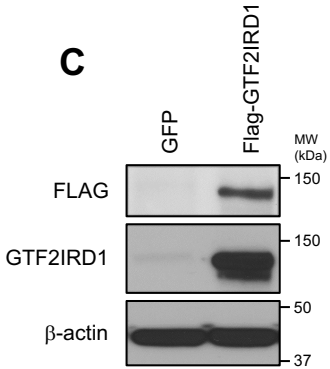
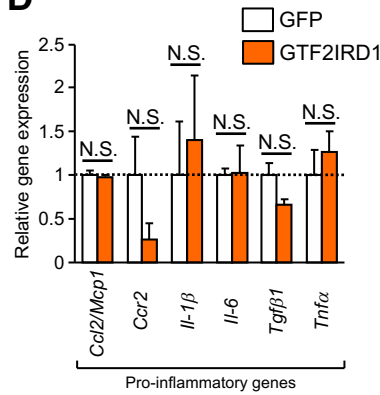
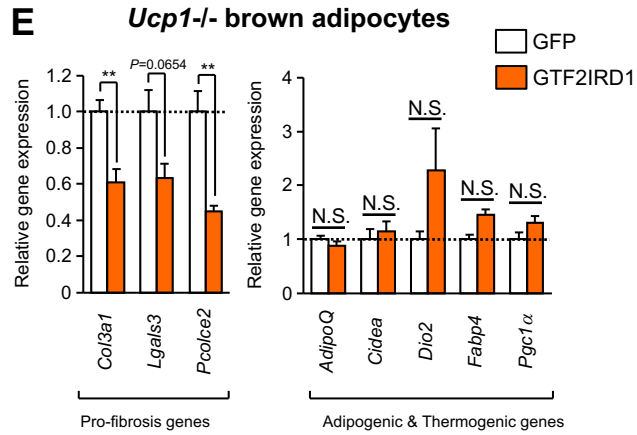
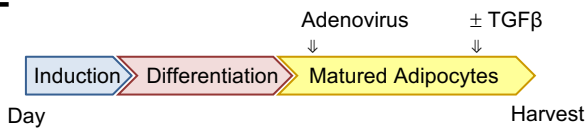
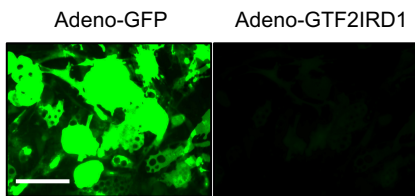
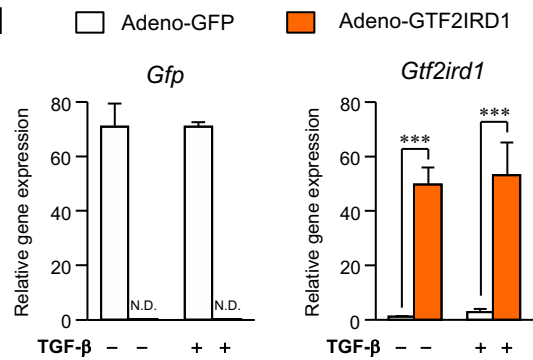
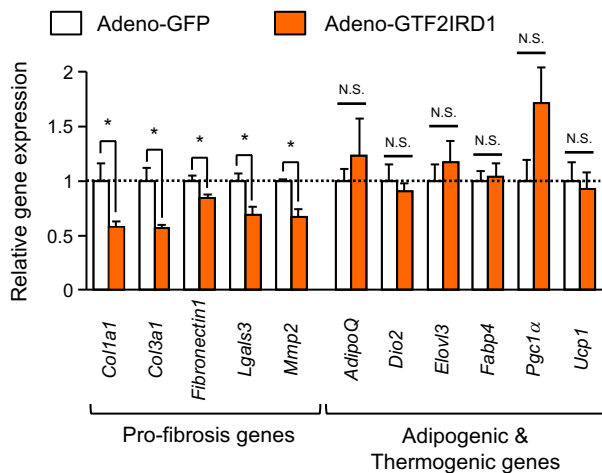
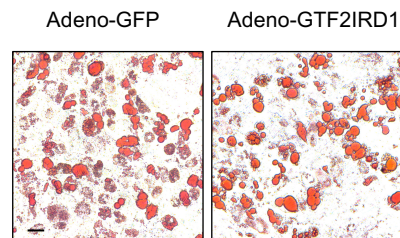
Supplementary Fig. 2 (related to Figure 3): Fat-selective transgenic expression of *Gtf2ird1* reduced adipose tissue fibrosis without affecting thermogenesis *in vivo*.

- (A) Relative mRNA expression of *Gtf2ird1* in indicated tissues from *Gtf2ird1* Tg mice and the littermate controls. ** $P < 0.01$. n=3. N.S., not significant.
- (B) Western blotting for GTF2IRD1 protein in the inguinal WAT. β -actin was used as loading control. Molecular weight (kDa) is shown on the right.
- (C) Relative mRNA expression of the indicated genes in the BMDMs isolated from *Gtf2ird1* Tg mice or the littermate controls treated with vehicle, IL4, SA, PA, or LPS. n=4.
- (D) Relative mRNA expression of the thermogenic genes in the BAT from *Gtf2ird1* Tg mice and the littermate controls after 18 weeks of high-fat diet. n=6-7.
- (E) Relative mRNA expression of the thermogenic genes in the BAT of *Gtf2ird1* Tg mice and the littermate controls under ambient temperature (22°C) and cold (6 °C) for 8 hours.
- (F) Relative mRNA expression of the creatine futile cycle genes in the inguinal WAT of *Gtf2ird1* Tg mice and the littermate controls after 11 weeks of high-fat diet. n=6-7.
- (G) Relative mRNA expression of the creatine futile cycle genes in the inguinal WAT of mice with indicated genotypes on a HFD for 14 weeks. n=3.
- (H) Heat production (Kcal h⁻¹) in individually housed *Gtf2ird1* Tg mice and the littermate controls at indicated temperature. n=5-6. N.S., not significant. Quantitative data are expressed as means \pm SEM.



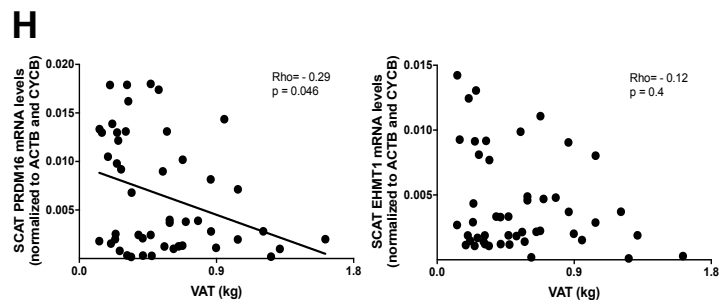
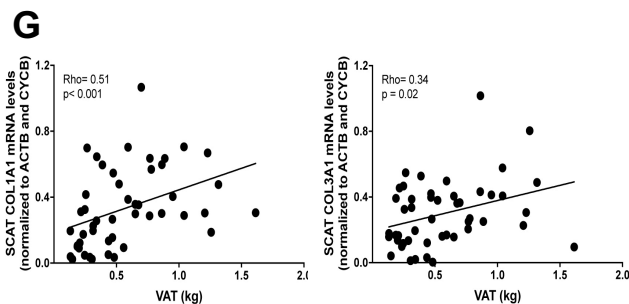
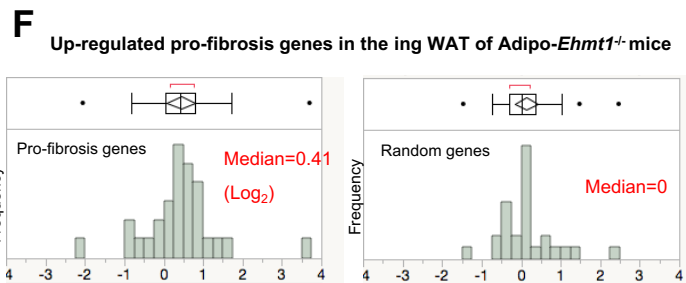
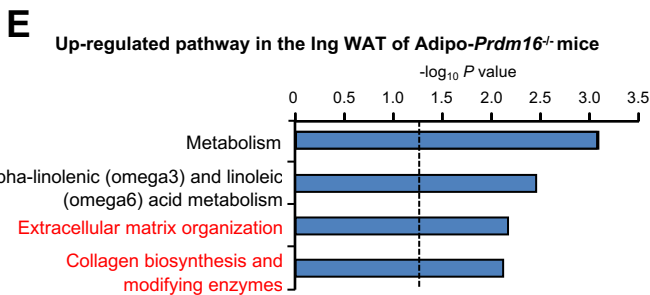
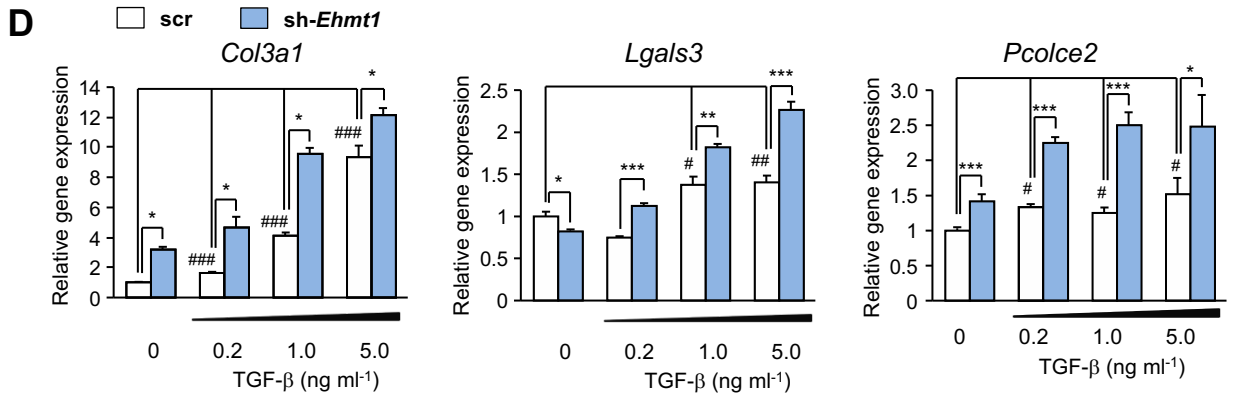
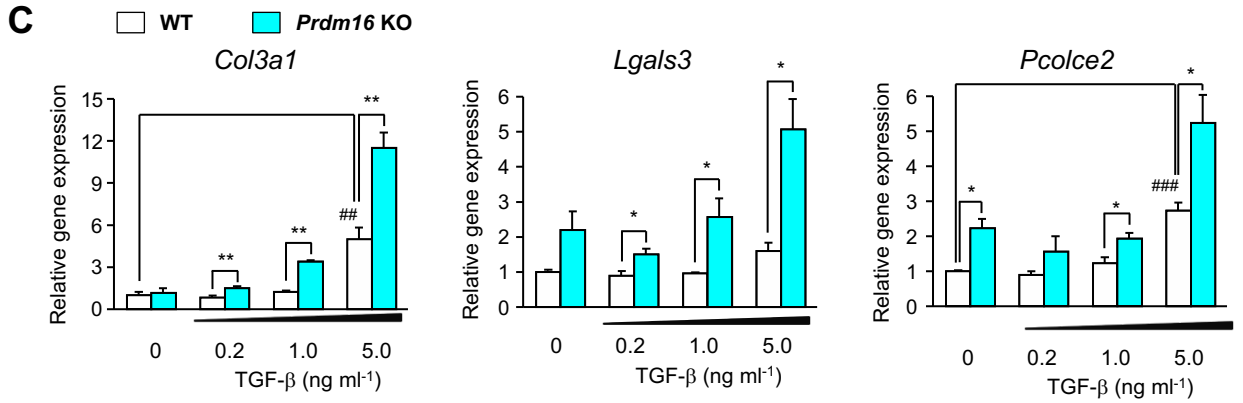
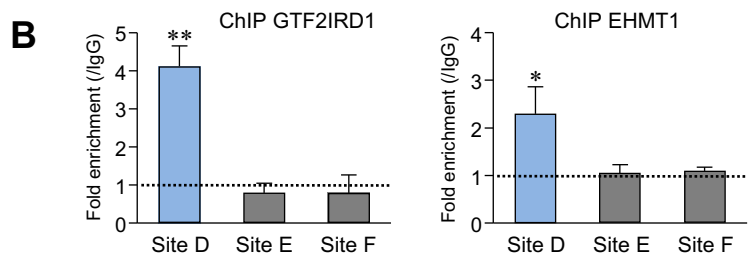
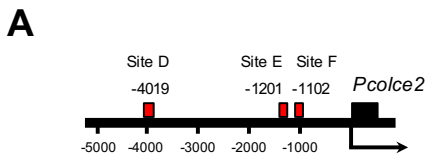
Supplementary Fig. 3 (related to Figure 3): Fat-selective transgenic expression of *Gtf2ird1* reduced adipose tissue fibrosis without affecting lipogenesis/lipolysis *in vivo*.

- (A) Picosirius staining in the BAT, the inguinal WAT and the epididymal WAT from *Gtf2ird1* Tg mice and the littermate controls on a regular diet (RD) and HFD for 11, 18 and 24 weeks. Scale bars = 100 μ m.
- (B) Repressed biological pathways in the epididymal WAT of *Gtf2ird1* Tg mice relative to the littermate controls. Analysis was performed by Metascape. $P < 0.05$.
- (C) Relative mRNA expression of the lipogenic and lipolysis genes in the BAT (left) and the inguinal WAT (right) from *Gtf2ird1* Tg mice and the littermate controls. $n = 5-6$. N.S., not significant. Data are expressed as means \pm SEM.

A**B****C****D****E****F****G****H****I****J**

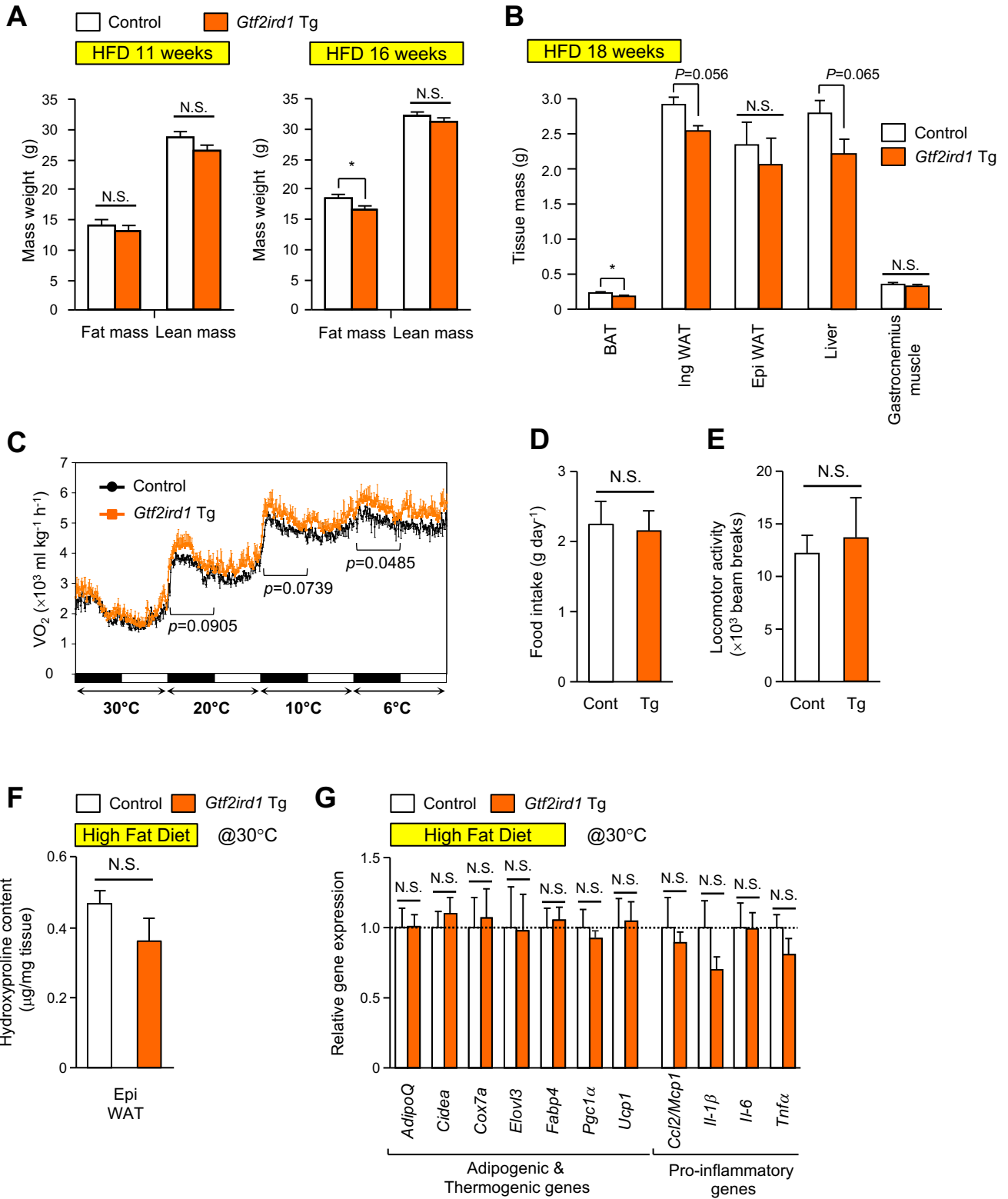
Supplementary Fig. 4 (related to Figure 4): Regulatory mechanisms of adipose tissue fibrosis by GTF2IRD1.

- (A) Relative mRNA expression of pro-fibrosis genes by qRT-PCR. * $P < 0.05$, *** $P < 0.001$ between scrambled control and sh-*Gtf2ird1*. ## $P < 0.01$ between vehicle and TGF- β . n=4.
- (B) Relative mRNA expression of pro-inflammatory genes in immortalized brown adipocytes expressing scr or sh-*Gtf2ird1*. Cells were treated with TGF- β to induce fibrosis. n=4. N.S., not significant.
- (C) Western blotting for indicated proteins in immortalized brown adipocytes expressing GFP or GTF2IRD1. β -actin was used as loading control.
- (D) Relative mRNA expression of pro-inflammatory genes in immortalized brown adipocytes expressing GFP or GTF2IRD1. Cells were treated with TGF- β to induce fibrosis. N.S., not significant.
- (E) Relative mRNA expression of pro-fibrosis genes (left) and adipogenesis and thermogenesis genes (right) in *Ucp1*^{-/-} brown adipocytes expressing GFP control or GTF2IRD1. ** $P < 0.01$, *** $P < 0.001$ between control GFP and GTF2IRD1. n=4. N.S., not significant.
- (F) Experimental design to determine the effect of GTF2IRD1 overexpression on differentiated primary adipocytes. Primary SVFs were differentiated under an adipogenic condition and subsequently infected with adenovirus expressing GFP or GTF2IRD1.
- (G) Microscopic image of the differentiated inguinal WAT-derived primary adipocytes expressing GFP or GTF2IRD1. Note that GTF2IRD1 virus does not contain GFP. Scale bar, 100 μ m.
- (H) Relative mRNA expression of *Gfp* (left) and *Gtf2ird1* (right) in (G). *** $P < 0.001$ between GFP control and GTF2IRD1. N.D., not detected.
- (I) Relative mRNA expression of pro-fibrosis genes, adipogenic and thermogenesis genes in differentiated adipocytes expressing GFP or GTF2IRD1. Cells were treated with TGF- β to induce fibrosis. * $P < 0.05$ between GFP control and GTF2IRD1. n=4. N.S., not significant.
- (J) Oil-red-O staining of differentiated adipocytes in (I). Scale bar, 100 μ m.



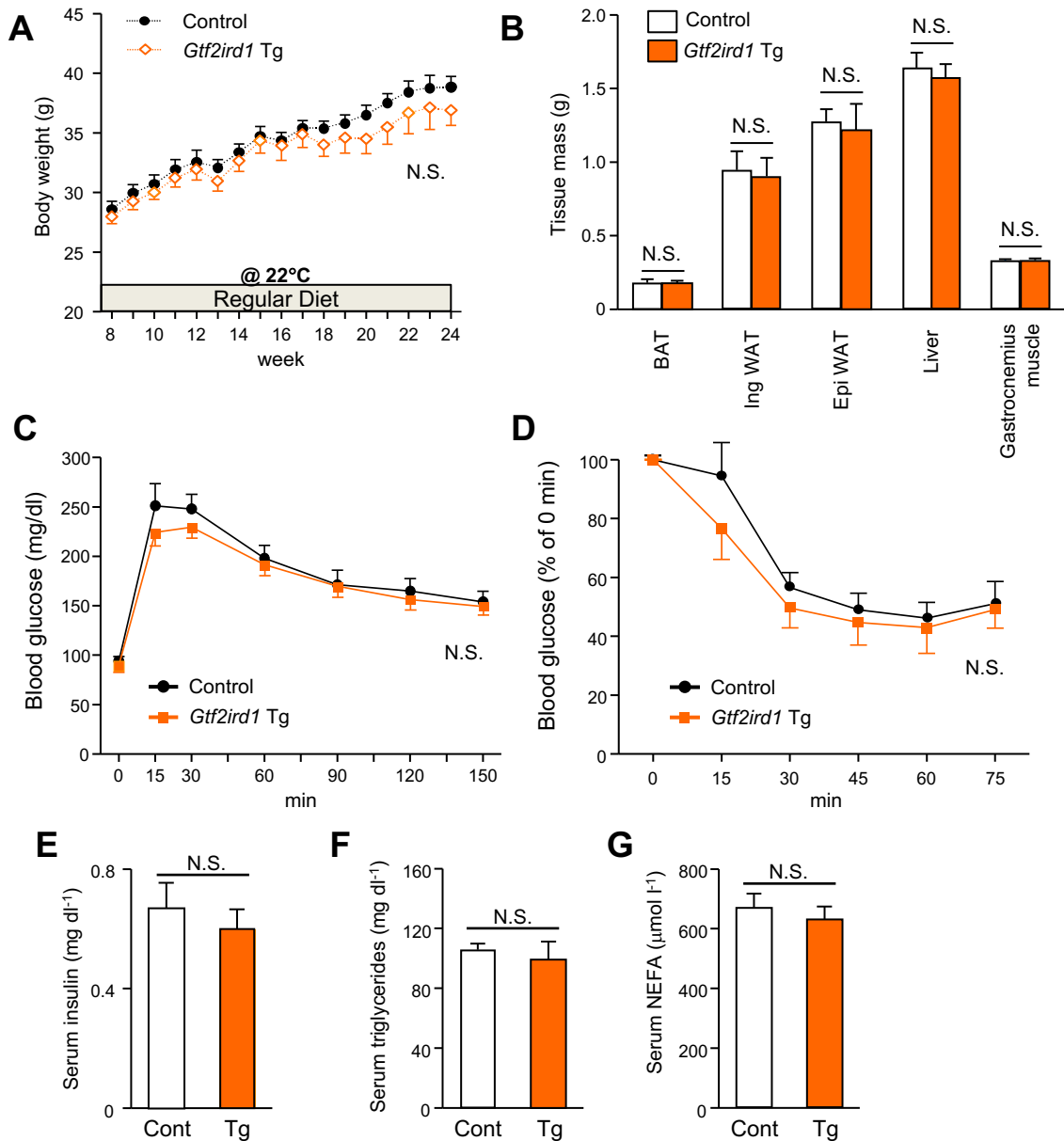
Supplementary Fig. 5 (related to Figure 5): Repression of adipose tissue fibrosis by GTF2IRD1 is mediated through a PRDM16-EHMT1 transcriptional complex.

- (A) Location of GTF2IRD1 binding motifs on the promoter/enhancer regions of *Pcolce2* (Site D-F) .
- (B) Chromatin immunoprecipitation assays in brown adipocytes using specific antibodies against GTF2IRD1 and EHMT1. Fold enrichment at each GTF2IRD1 binding motif site in (A) was assessed by qPCR compared to IgG control. * $P < 0.05$, ** $P < 0.01$, $n = 3$.
- (C) Relative mRNA expression of pro-fibrosis genes in the WT and *Prdm16*^{-/-} brown adipocytes. Cells were treated with TGF- β at indicated doses. * $P < 0.05$, ** $P < 0.01$ between WT and *Prdm16*^{-/-} adipocytes. ## $P < 0.01$, ### $P < 0.001$ between vehicle and TGF- β at indicated doses. $n = 4$.
- (D) Relative mRNA expression of pro-fibrosis genes from immortalized brown adipocytes expressing scr and sh-*Ehmt1*. Cells were treated with TGF- β at indicated doses. * $P < 0.05$, ** $P < 0.01$, *** $P < 0.001$ between scrambled control and sh-*Ehmt1*. # $P < 0.05$, ## $P < 0.01$, ### $P < 0.001$ between vehicle and TGF- β at indicated doses. $n = 4$.
- (E) Up-regulated biological pathways in the inguinal WAT of Adipo-*Prdm16*^{-/-} mice relative to the littermate controls. Analysis was performed by Metascape.
- (F) Expression profile of the pro-fibrosis genes, listed in the Figure 1E (left) and random genes (right), representing the frequency of Z scored FPKM in the inguinal WAT of Adipo-*Ehmt1*^{-/-} mice.
- (G) Relative mRNA levels of two additional pro-fibrotic genes, *COL1A1*, *COL3A1* in the abdominal subcutaneous WAT of 48 adult human subjects, showing a correlation with visceral adipose tissue (VAT) mass, as measured by DEXA.
- (H) Relative mRNA levels of PRDM16 and EHMT1 in the abdominal subcutaneous WAT of 48 adult human subjects, showing a correlation with visceral adipose tissue (VAT) mass.



Supplementary Fig. 6 (related to Figure 6): Metabolic phenotypes of *Gtf2ird1* Tg mice on a HFD.

- (A) Fat and lean mass of *Gtf2ird1* Tg mice and the littermate controls after 11 weeks (left) and 16 weeks (right) of HFD by Echo-MRI. n=6-7. * $P < 0.05$ between *Gtf2ird1* Tg mice and the littermate controls. N.S., not significant.
- (B) Weight of the indicated tissues from *Gtf2ird1* Tg mice and the littermate controls after 18 weeks of HFD. * $P < 0.05$ between *Gtf2ird1* Tg mice and the littermate controls. n=6-7. N.S., not significant.
- (C) Whole-body energy expenditure (VO_2) in individually housed *Gtf2ird1* Tg mice and the littermate controls on a HFD for 8 weeks at indicated temperature. n=5-6.
- (D) Food intake in *Gtf2ird1* Tg mice and the littermate controls by CLAMS in (C).
- (E) Locomotor activity (beam breaks) in *Gtf2ird1* Tg mice and the littermate controls by CLAMS in (C).
- (F) Relative mRNA expression of adipogenic/thermogenic genes and pro-fibrosis genes in *Gtf2ird1* Tg mice and the littermate controls after 12 weeks of HFD under thermoneutrality. n=6-7. N.S., not significant. Quantitative data are expressed as means \pm SEM.



Supplementary Fig. 7 (related to Figure 6): Metabolic phenotype of *Gtf2ird1* Tg mice on a RD.

- (A) Body-weight gain of *Gtf2ird1* Tg mice and the littermate controls on a RD at ambient temperature. n= 6-9. N.S., not significant.
- (B) Weight of the indicated tissues from *Gtf2ird1* Tg mice and the littermate controls on a RD. n=6-7. N.S., not significant.
- (C) Glucose tolerance test in *Gtf2ird1* Tg mice and the littermate controls on a RD at 18 weeks old. n=6. N.S., not significant.
- (D) Insulin tolerance test in *Gtf2ird1* Tg mice and the littermate controls on a RD at 18 weeks old. n=6. N.S., not significant.
- (E) Serum concentrations of fasting insulin in *Gtf2ird1* Tg mice and the littermate controls. n=6-7. N.S., not significant.
- (F) Serum level of triglycerides in mice in (E).
- (G) Serum level of NEFA in mice in (E). All the data are expressed as means \pm SEM.